Climate-Catchment-Soil Control on Hydrological Droughts in Peninsular India

Poulomi Ganguli[1,*,#], Bhupinderjeet Singh[1,#], Nagarjuna N. Reddy[1], Aparna Raut[1], Debasish Mishra[1], Bhabani Sankar Das[1]

[1]Agricultural and Food Engineering Department, Indian Institute of Technology Kharagpur, West Bengal, Kharagpur 721302, India

[*]Corresponding Author: pganguli@agfe.iitkgp.ac.in

[#]These authors contributed equally to this work.

Abstract

Most land surface system models and observational assessments ignore detailed soil characteristics while describing the drought attributes such as growth, duration, recovery, and the termination rate of the event. With the national-scale digital soil maps available for India, we assessed the climate-catchment-soil nexus using daily observed streamflow records from 98 sites in tropical rain-dominated catchments of peninsular India (8 - 25° N, 72 - 86° E). Results indicated that climate-catchment-soil properties may control hydrological drought attributes to the tune of 14-70%. While terrain features are dominant drivers for drought growth, contributing around 50% variability, soil attributes contribute ~71.5% variability in drought duration. Finally, soil and climatic factors together control the resilience and termination rate. The most relevant climate characteristics are potential evapotranspiration, soil moisture, rainfall, and temperature; temperature and soil moisture are dominant controls for streamflow drought resilience. Among different soil properties, soil organic carbon (SOC) stock could resist drought propagation, despite low-carbon soils across the Indian subcontinent. The findings highlight the need for accounting feedback among climate, soil, and topographical properties in catchment-scale drought propagations.

Introduction

Peninsular River Basins (PRB) of India (8-25° N, 72-86° E) are facing increasingly severe droughts and water scarcity[1–3]. Climate change and an ever-growing population further strain locally-available surface water[4] gradually push the region towards a 'day-zero' situation[5]. Krishna and Godavari are the two major rivers in PRB and both are rain-fed. Failures and delays in southwest (June to September) or northeastern (October – December) monsoon[6–8] in this region trigger below-normal streamflow and hydrological droughts[9] in varying intensities. Even with decades of catchment-scale drought propagation studies[2,8,12,11,12], it is not clear how a given river basin develops into a "drought-rich" or "drought-poor" region. Climate and catchment control on hydrological droughts are more or less known[13–17]; however, no studies have attempted to examine how varying soil conditions influence these controls. With the availability of a national-scale digital soil map[18], here we explore the climate-catchment-soil control on hydrological droughts and identify key drought drivers (KDD) for drought propagation.

We used daily observed streamflow records of past 50 years (1965 – 2019) from 98 stream gauges over PRB in a multi-stage framework[19,20] (**Fig. 1**) to quantify the contiguity in locations and time of occurrence of hydrologic droughts (the space-time clustering[21] or synchronicity in drought properties) and identify potential KDDs from a wide range of climate, soil, and terrain attributes (**Fig. 1**, Supplementary **Fig. S1**, **Table S1**). We applied a daily variable threshold approach to derive streamflow droughts by developing 366 (additional for leap year) flow duration curves using continuous streamflow records[22] (Methods). While we obtain meteorological and catchment-specific geospatial attributes from the archived database[23–27], the soil attributes are derived from a recently developed digital soil database of India[18] (see Data and Method section). We show the extent to which climate, catchment and soil attributes influences and co-vary with catchment-scale drought characteristics (Methods), such as growth, persistence (duration and frequency or number of events), recovery, and drought termination rate (DTR). Specifically, we investigate how soil organic carbon (SOC) influence the growth, persistence, and recovery of droughts over PRB given that the Indian soils are typically low in SOC contents[18,28].

Space-Time Synchronicity in Drought Responses

Previous studies[10-13,29] have used gridded hydrometeorological forcing with a coarser temporal resolution to identify drought clusters over PRB. Here, we identify the temporal evolution of drought characteristics using continuous daily streamflow records, namely, drought growth, persistence, recovery and the DTR (See Methods; **Fig. 1b-c**). Then, we identify drought regimes by applying a clustering algorithm to 98 gauges across PRB based on 9 catchment-scale drought attributes (see Methods): (i) latitude and longitude of the stream gauges; (ii) drought properties, *i.e.*, mean and maximum drought duration, and mean and maximum deficit volume; (iii) catchment properties, such as the baseflow index (BFI)[30] and catchment area, and (iv) seasonality[31] in drought termination. We show the temporal evolution of drought characteristics and identify the presence of "drought rich" and "drought poor" periods over the past five decades using the Hovmöller diagram (**Fig. S2**). The decadal pattern of events (during the time-window 1979-80, 1989-90, 2001-02, 2008-10) shows over 30% of the areas are drought-affected. Further, we identify spatial clustering of persistent droughts over several regions, primarily concentrated between latitudinal belts 13° and 20°N latitudes between 2001 to 2005, including two major historical hydrological drought events spanning the periods, 2000-01 and 2003-04 (ref. [10]). The drought in 2000 is mainly attributed to warmer Sea Surface Temperature (SST) conditions that drive warm El Niño conditions in the Pacific and Indian oceans[10]. An earlier study[32] reported a decrease in precipitation and low seasonal streamflow variability over PRB is associated with the warm El Niño Southern Oscillation (ENSO) episode. On the other hand, drought in July 2002 was typically associated with the lack of monsoon rainfall, which led to droughts in a large part of the western peninsula[33].

To explore the nature of hydrological drought responses on a regional scale, we delineate the collection of sites based on fuzzy c-means clustering[34,35] (see Methods and the Supplementary Information SI 1.2). A study by Ahmadi et al.[20] showed characterizing droughts into different stages or properties provide better understanding of temporal and spatial coherence of localized drought events. Further, Yaeger *et al.*[36] showed that only accounting geomorphological features and drought attributes may not provide a credible estimate of the homogenous region. Hence, we introduce the seasonality of drought termination month, represented by the mean date of drought termination, to identify homogenous regions (see Methods). The regionalization of hydrological droughts based on drought properties involves the Principal Component Analysis (PCA) followed by fuzzy c-means clustering method[37] (See SI 1.2). Based on PCA and fuzzy clustering, we identify the optimal number of drought regimes (*i.e.*, represented by a cluster of sites based on drought-specific attributes) as 4. We find that collectively the first six principal components (PCs) explain the ≈94% variability of the streamflow droughts characteristics (**Fig. S3a**); therefore, only the first six PCs are used for identifying drought clusters. The biplot of the top two PCs of the selected attributes shows (**Fig. S3b**) that the maximum and mean drought durations have notable contribution to the first PC. On the other hand, for the second PC, the seasonality of drought termination, showed the significant contribution. The mean deficit volume and the catchment area did not significantly contribute to the first two PCs. The BFI showed a negative correlation with both these PCs. Geospatial locations and drought durations significantly contributed to the spatial variations in clusters 1 and 4 and the mean termination date contributed to the spatial variations in cluster 2. Finally, the BFI that inherently embeds the effect of geology and soil permeability is the major contributor for variations in cluster 3.

Fig. 2a shows the delineated hydrological drought regimes, a large fraction of stream gauges located across the central part of PRB is under regime 1 with 35% spatial extent; whereas regimes 2-4 contain 20-24% of gauges. **Figs. 2b-f** shows the spatial distribution of drought characteristics during 1965-2018 time window. Most catchments located in Central (*i.e.*, catchments of Godavari, and Narmada) and a few of eastern (Subarnarekha and Mahanadi) river basins (**Fig. S1**) reported a large growth period, often more than a week (**Fig. 2b**) with frequent drought (**Fig. 2f**) events. The average drought duration in the catchments of Godavari and Narmada from regimes 1 and 2 ranges more than 50 to 100 days. In particular, the catchments in regime 1 show a large variation in DTR often exceeding 250 mm/day (**Fig. 2d**) with a recovery length more than a month (**Fig. 2e**). The spatial distribution of seasonality in drought termination (**Fig. S4**) shows high regularity in drought termination for regimes 1 and 2 with average seasonality of more than 0.5. The catchments in regime 1, which includes 74% sub-basins from Narmada, and the Godavari in Central India and remaining from Krishna, and Mahanadi basins contains large watershed area and show persistently longer drought episodes with average termination period during mid-monsoon season during the month of September. Temporal evolution of drought characteristics during 2000 – 2005 time window for rivers in Central India (regime 1) shows (**Fig. S5**) the growth of droughts initiated during the month of August in 2000, which lasted until early 2001; subsequently, the majority of stations showed recovery in the monsoon season of the same year (i.e., in June 2001). During the year 2003 – 05, we note the presence of multi-season persistent droughts, especially towards the South of 20°N, which lasted for more than a year (from March 2004 to July 2005) in this region. The rivers in this region contains low BFI with a median value around 0.3. Further, this region often accompanied by strong local heating of the black soils with high PET[38], which could lead to low baseflow yield in this region[39]. The low BFI, indicates a flashy flow regime with less permeable soil that may generate more minor drought events that have short duration.

The sub-basins in Regime 2 shows relatively fewer drought events than other regions with relatively low average drought duration (less than 100 days; **Fig. 2c**) and is associated with the lowest average recovery period (average recovery less than a month; **Fig. 2e**). This regime includes 70% of sub-basins from Krishna, Tapi, and the Godavari River basins (**Fig. S1**) with moderately large catchments areas. The most severe drought that occurred in Regime 2 lasted around 250 days (August 2003 to April 2004; **Fig. S5**). For gauges located in this regime, the drought terminations ranges between August and December months with median termination during post-monsoon season in October (**Fig. S4**). The values of BFI tend to be the lowest for this regime as compared to others, with a median BFI value of 0.25 (**Fig. S4**). Interestingly, the rivers in this regime shows a strong seasonality in the mean timing of drought termination with the strength of seasonality close to 0.8 indicating high persistence in drought termination, i.e., all streamflow droughts at a particular site occur on the same day of the years during the analysis time window[40].

Regime 3, comprising nearly 60% of sub-basins from Cauvery and Krishna and the rest from the southern peninsula region (*e.g.,* Pampa, Periyar, Vaigai), experience the lowest number of droughts (on an average, 15-20 events; **Fig. 2f**) followed by a minimum variation in the DTR (< 15 mm/day; **Fig. 2d**). In general, the drought termination pattern in regime 3 does not show any specific trend with termination period scattered throughout the year with a large variation in seasonality strength; however, August is detetect as the median termination month (**Fig. S4**). The rivers in this regime shows the highest BFI (with BFI > 0.5), which may be due to the presence of large reservoirs (the Krishnaraj Sagara reservoir over Cauvery River) and wet lands[41,42]. The catchments with high BFI sustain the recharge and groundwater storage[39], which results in large variation in drought termination months (or low seasonality in drought termination; **Fig. S4)**.The analysis of 2000-05 time window for regime 3 shows (**Fig. S5**) the "drought-rich" periods exist after 2002, which persists between 2003 and 2005. By early 2003, the catchments of Cauvery and a few catchments in southern India (*e.g.,* Pampa and Ponnaiyar) were also affected and remained under drought throughout the year, which recovered later in April-May 2004.

Finally, regime 4, comprising a majority of catchments across eastern peninsular India (87% of sub-basins from Mahanadi, Subarnarekha, and Brahmani and the rest from Baitarni and Godavari; **Fig**. **S1**) reported an average drought duration of more than two months with a large variability in drought frequency (15-30 events) (**Fig. 2f).** The average drought recovery length in this regime is relatively larger (**Fig. 2e**) and a large number of sites show recovery period more than 40 days. The most severe drought in regime 4 occurred in August 1979 which lasted until July 1980 (**Fig. S2**) and was considered as a severe drought in the literature[43,44]. The average drought termination period in this regime is mainly during post-monsoon period in November (**Fig. S4**) with termination months varies from October to December. The catchments in this regime showed the least regularity in drought termination (Fig. S4).

Overall, our analyses reveal the following: (*i*) majority of regimes (1, 2, and 4) show the average termination either in the monsoon (June-September) or post-monsoon (October-December) months suggesting profound roles of southwest and northeast monsoon rainfalls in the termination of droughts. On the other hand, regime 3 showed no specific trend in drought termination seasonality with termination periods scattered throughout the year. (*ii*) Large spatial heterogeneity in drought responses indicates drought stages differ significantly across space and time, which could be a consequence of several factors including topography and morphological attributes of catchments, soil, and climatic controls[15,16,45].

Hot and Cold Spots of Streamflow Droughts

To further explain the nature of synchronicity in drought responses and identify vulnerable regions, we compare the maximum deficit volume and maximum duration of streamflow droughts (**Fig. 3a**). In addition, we present heat maps of drought deficit volume-recurrence interval-vs-recovery duration for different regimes (**Fig. 3b**). A large fraction of gauges in Regime 1 is characterized by moderately severe drought (a spatial average value of 1.7 mm); however, experiences long and persistent drought episodes (more than 250 days; **Fig. 3a**). The rivers in this regime show an extended drought recovery period coinciding with a short return time or recurrence interval (within the range of 250 days; **Fig. 3b**).

On the other hand, regime 2 shows droughts with relatively longer recurrence interval accompanied by more than a month of recovery period. Droughts in this regime have the lowest deficit volume with average deficit volume ~0.74 mm (**Fig. 3a** and **b)**. This could be because catchments in this region show the lowest BFI values than others (**Fig. S4)**, suggesting a minimum contribution towards groundwater recharge owing to relatively impermeable geology[16, 46-47]. Regime 3 shows the largest average recovery length (**Fig. 2e**) with considerable variability in deficit volume – a few outlying events even led to deficit volume of more than 200 mm (See whisker length of the box plot in **Fig. 3a**). This region also shows considerable variability in drought seasonality (**Fig S4**). Interestingly, more than 50% of sites show a recovery period of less than a month (shades of the pixels in **Fig. 3b**) with an average recurrence interval of 350 days (**Fig. 3b**), which is the largest among all regimes. A relatively small recovery period compounded by a large recurrence interval could be due to the largest baseflow indices of catchments in this region (**Fig. S4**), which indicate relatively permeable geology with substantial groundwater recharge.

Finally, regime 4 shows a contrasting pattern to regime 1, where droughts with relatively less deficit volume (< 1 mm) are coincided with a recovery period of more than a month. Further, a rare event characterized by a high deficit volume of more than 10 mm and a prolonged recurrence interval of more than 100 days often witnesses a low recovery period (typically less than a month; **Fig. 3b,** *bottom right corner*). A relatively long recovery period could be because of low baseflow indices for gauges in this region with a median value of less than 0.5 (**Fig. S4**), indicating a flashy river basin[47,49] analogous to regime 2.

Overall, our analysis shows the following: (*i*) catchments in central peninsular India (13-23°N and 73-84°E) is exposed to frequent droughts compounded by a long recovery period, making it one of the most vulnerable regions where a chronic state may be reached when an incomplete recovery would coincide with another severe drought episode leading to an adverse consequence to land-carbon sink. Interestingly, this region contains relatively low SOC contents as may be seen in the newly developed national SOC map[18]. (*ii*) In contrast, catchments in regime 2 are characterized by relatively less severe droughts with a larger recovery period despite having the lowest BFI in regime 2. We hypothesize that streamflow drought resiliency in regime 2 could be partially linked to the high SOC content of the soil in the Western Ghat area of the PRB[18] - a high SOC may lead to an increase in soil water storage capacity resulting in a slowdown in severe drought occurrences. On the other hand, the low BFI at region 2 could be associated with climate, soil and geomorphologic properties. While soil controls the infiltration of water, the underlying aquifer properties control the storage and release of water to streams. Recently, Naveena *et al.*[38] have detected emergence of a "hot blob" during the pre-monsoon season (end of March – May) over the south-central parts of the PRB, which promotes the accumulation of high temperature in this region. High clay content of black soils (region 2) further abets the sustenance of the "hot blob" resulting in higher frequencies of hot days, which could lead to low baseflow yields in this region[39].

Key Drought Drivers (KDD's) Influencing Drought Vulnerability

To provide a causal attribution of drought responses, we investigate the influence of several covariates, such as meteorological variables, soil properties, and catchment-specific terrain attributes (**Table S1**), totaling 89 hydrometeorological and morphological features. The Shapiro-Wilk test of drought variables as well as the covariates reveal that 85% of variables (*i.e.*, 79 out of 93) show a strong deviation from normality assumption at a 10% significance level. The skewness and kurtosis values of covariates further confirm that the covariates exhibit a strong asymmetry (**Fig. S7**). The nonparametric dependence analysis (Kendall's τ test) suggests that the drought growth strongly depends on (significant positive dependence) terrain features in regime 1, from which topographic wetness index (TWI) shows the highest correlation value of Kendall's $\tau = 0.39$. This could be because the TWI[50,51], which is a function of the local slope with the upslope contributing area per contour length, will be more likely in wet and relatively shallow soils with moderate slopes, where soil permeability increases with saturation. On the other hand, drought duration and recovery show (significant) negative dependence on SOC and stock (Kendall's $\tau < -0.21$). This may be due to moderately low SOC content in this region[18,28].

In regime 2, the drought growth shows positive dependence to both soil and meteorological attributes, such as the mean temperature of April-July (Kendall's $\tau > 0.48$) followed by pH and cation exchange capacity (CEC) values at 0.3 and 1 m soil depths (Kendall's $\tau > 0.47$), respectively, whereas a negative dependence was observed for SOC content and SOC stock (Kendall's $\tau < -0.35$). In contrast, the recovery stage in this region shows more dependence on terrain features. In regime 3, the growth shows a strong positive dependence on different soil moisture covariates (**Fig. S7**). Further, there is high variability among factors influencing drought duration and recovery – in general, sub-basins show a strong negative dependence on soil organic content (Kendall's τ < -0.44). In contrast, DTR fails to show any conclusive evidence of significantly strong dependence on any of the covariates. Finally, in regime 4, recovery and DTR show a moderately strong dependence with meteorological and terrain features, which is in the order of ± 0.4 (*i.e.*, terrain feature slope show a significant negative dependence with drought recovery, Kendall's $\tau_{recovery}$ = -0.4 and a significant positive correlation with DTR, Kendall's τ_{DTR} = 0.38).

Our analyses reveal a large proportion of gauges in regimes 2 and 3 that show a strong dependence on covariates. For example, in regime 2, 51% of catchments show strong dependence with covariates during growth phases. Likewise, drought persistency in regime 3 is largely controlled by 65% of covariates. Further, the drought resilience or recovery phase in regime 3 is more strongly influenced by terrain features as reflected by the largest BFI values followed by meteorological attributes. On the other hand, in regime 2 recovery phase shows a strong positive correlation, associated with terrain features. As noted earlier, the sub-basins in regime 2 show the lowest BFI indicating a minimum baseflow contribution or groundwater replenishment, which results in a relatively long recovery period in this region. Our results corroborate with an earlier studies[48,49,52], which showed low flows are often controlled by the soil and geology of the catchment.

We employed a hybrid feature selection procedure consisting of filtering and wrapping through Boruta algorithm[53] (see Methods) using all 89 covariates. The average sand contents at 1 m depth in the western part of the peninsula is relatively low as compared to the eastern and southern part of the peninsula, which influences the drought growth for gauges in this region (**Fig. S8a**), whereas a relatively high clay content in this region affects average drought termination rate (**Fig. S8d**). The SOC content and SOC stock at 1 m depth over a large portion of the landmass is consistently low (**Fig. S8b-c**). Among three KDD categories (soil, hydro-meteorological and terrain), drought growth appears to be most influenced by ~ 17% (15 out of 89) attributes (see **Fig. 4a**), *e.g.*, the cross-sectional (Kendall's τ = -0.23) and longitudinal (Kendall's τ = 0.22) curvatures, slope (Kendall's τ = -0.23), and terrain roughness index (Kendall's τ = -0.23) in addition to sand content (Kendall's τ = - 0.14), CEC (Kendall's τ = 0.20), and soil moisture for the months of January (Kendall's τ = - 0.18), April (Kendall's τ = - 0.19), and May (Kendall's τ = -0.21), denoting the influence of soil moisture on drought growth in the transition months from winter to spring and spring to summer. Drought growth shows a strong dependence on hydro-meteorological factors, such as average potential evapotranspiration (PET) at the onset (Kendall's τ = 0.14 for June) and retrieval (Kendall's τ = 0.17 for September) months of monsoon. This could be because of feedback between soil moisture and surface water availability (precipitation minus evapotranspiration, *P-E*). In water-limited regions, the soil moisture is shown to modulate evapotranspiration, which positively feedbacks precipitation via moisture recycling[54,55]. The drought duration showed strong dependence on soil properties, primarily SOC and SOC stock and mean monthly winter (November - December) soil moisture and temperature regimes. However, no terrain features are found to be critical in influencing drought duration. In general, soils with low SOC contents and moisture deficits during post-monsoon seasons will have a longer drought duration. Likewise, drought recovery appears to be largely dependent on mean monthly soil moisture contents during February and March (Kendall's $\tau = 0.12$), mean temperature of February (Kendall's $\tau = -0.17$) and January (Kendall's $\tau = -0.18$), SOC contents, and SOC stocks of top 1 m soil profile (Kendall's $\tau = -0.21$). This agrees qualitatively with findings from an earlier study[56], which showed that temperature strongly influences streamflow-based drought characteristics such as spatial extent and duration. Further, SOC controls the soil moisture levels and, in turn, drought development and termination stages (**Fig. S8**)[28,57].

Interestingly, **Fig. 4b** confirms that the early monsoon (June-July) soil moisture conditions and winter (primarily between November and December) temperature notably impact on drought duration. On the other hand, drought recovery heavily depends on the soil moisture regime during the spring (February-March) and the temperature conditions during the winter (November-January) until the end of the spring (March-end) season. Likewise, the DTR is typically influenced by only 12% (11 out of 89) attributes (**Fig. 4d**). An apparent positive dependence between PET (Kendall's $\tau = 0.17$), clay content (Kendall's $\tau = 0.16$), and CEC (Kendall's $\tau = 0.14$) with DTR suggests the inherent ability of soils coupled with hydro-meteorological factors to accelerate or cease prevailing desiccation. These are further aided by terrain factors such as flow accumulation (Kendall's $\tau = 0.22$) and relative slope (Kendall's $\tau = 0.18$) in the governing rate of drought termination. Overall, our results show that drought growth is largely controlled by terrain attributes ~50% of total covariates; drought persistently is mostly controlled by soil attributes accounting for more than 70% of all three covariates. Interestingly, drought recovery is equally controlled by hydroclimatic and soil properties with little or no role of terrain attributes, whereas DTR is primarily controlled by hydroclimatic (~51% share) and soil (~35% share) factors together.

Our analyses suggest the following: (*i*) Considering peninsular catchments as a whole, terrain features largely control drought growth; soil attributes contribute more than 70% in drought persistency; whereas DTR is largely controlled by meteorological attributes. In addition, drought resiliency is equally impacted by soil and meteorological attributes. (*ii*) Considering homogeneous drought regimes, a large proportion of gauges in regimes 2 and 3 show a strong dependence on growth (for regime 2) and persistent (for regime 3) phase, respectively. Further, drought recovery in regime 3 shows a strong anticorrelation with soil and terrain features, whereas a strong positive dependence on meteorological attributes, primarily with PET. The relatively small recovery period (less than a month) of most of the gauges compounded by a large recurrence interval at regime 3 could be attributed to the largest baseflow yields of catchments, which is largely controlled by geology, land use, catchment and terrain characteristics[16,48,49]. In addition, the meteorological factors, such as high evapotranspiration-induced moisture surplus accelerates a swift recovery. This clearly shows that soil, hydro-meteorological, and terrain features play distinct roles in the propagation of catchment-scale hydrological droughts.

Discussion and Conclusions

The observational evidence indicates strong support that heterogeneity in hydrological drought responses is controlled by feedback between climate-catchment-and-soil attributes (**Fig. 4** and **Fig. S7**). Previous studies[15,16,58,59] conducted on catchment-scale droughts provide important yet incomplete insights into the role of potential drivers in hydrological drought propagation. Based on an earlier study[60] that establishes structural control on catchment sensitivity, our approach further expanded on geomorphological features by exploring additional covariates, a range of terrain, and soil characteristics influencing various drought characteristics, which have not been investigated so far - neither in observational assessments nor in land surface model-based simulation[10,61]. The sources of uncertainty in the analyses stem from the quality of available records. Climate change may impart nonstationarity in low flow series, which may account for additional uncertainty in the analysis. However, we compensated this by considering average (or median) relationships, which is commonly applied in low flow regionalization studies and followed elsewhere[16] as a robust measure in presence of weak nonstationarity. Further, accounting nonstationarity in records would require longer hydroclimatic time series, which is limited for the area being considered here.

Our findings have direct implications for catchment-scale drought mitigation. The identified dynamic covariates, such as climate and soil moisture level could be utilized for monitoring drought stages one to two seasons advance and to support drought warning effort by developing a multivariate forecast model, enabling seasonal-to-sub-seasonal (S2S) prediction[62,63]. While meteorological to hydrological drought is forecasted at a monthly to the seasonal time scale in practice[64], timely issuance of targeted drought early warning systems (DEWS)[65] and a dynamical low flow forecast at a higher temporal resolution involving primary drought attributes, such as growth, persistence and recovery pattern, could be effective in mitigating impacts. Further, for climatologically heterogeneous regions of India, developing an improved probabilistic S2S low flow forecast integrating the static and dynamic controls could be of great interest in aiding economic resilience to droughts[66].

The obtained insights from this study highlight soil management plays a crucial role in desiccation and its resilience. Since climate variability and change have exacerbated the concurrence of warm-and-dry conditions[67], the persistence of carbon loss (the "legacy effect")[68] a few years after extreme and persistent droughts, may have long-term effects on the carbon-budget of the tropical rain-dominated ecosystem of the Indian peninsula. While soil carbon stocks for peninsular India are relatively low than that of the global average[28], efficient soil and water conservation measures can improve soil carbon sequestration[69,70] and enhance drought resilience, ensuring water-and-food security of the country[57].

Methods

Hydro-Meteorological Forcing Data Set

We obtain the observed daily streamflow time series from the nationwide water resources information system (India-WRIS; https://indiawris.gov.in/wris/). The observed streamflow records are obtained for the stations that are not considerably affected by major reservoirs and dams with an average ~16% (ranges from 3 – 33%) area under irrigations considering both surface and groundwater (*e.g.*, tube wells and dug wells) sources[71]. To ensure adequate spatial coverage as well as the completeness of records, we selected the catchments based on the following criteria: (1) The stations with a minimum of 20 years of continuous streamflow record availability during the analysis period (1965-2019); (2) The catchment area of the sub-basin to be at least 1000 km^2 or more. Based on this criteria, we selected 98 stream gauges with catchment area range between 1200 and 307,800 km^2 from 18 different river basins across PRB (**Fig. 1**; **Fig. S1**). Following the earlier literature[72,73], we infill the missing gaps in daily streamflow time series using the time series interpolation technique.

To examine meteorological control on drought stages, we use the observed gridded meteorological datasets with a spatial resolution of 0.5° available at a monthly time scale. The meteorological variables are precipitation[23], soil moisture (1.6 m depth)[26], mean air temperature (at a height 2 m above surface)[24], PET[25] estimated using the Penman-Monteith method. To identify potential KDDs for catchment-scale drought propagation processes, we obtain catchment boundaries from the Global Streamflow Indices and Metadata (GSIM) archive[27]. To ensure data compatibility, we kept the record lengths of hydrometeorological variables same as the streamflow record lengths for each catchment. Further, the baseflow index for each catchment is calculated following the WMO manual on low-flow estimation procedure[74].

Delineation of Drought Characteristics

We identify hydrological droughts by applying a variable threshold approach to the daily streamflow time series[15,19,22]. The advantage of using the variable threshold method of drought delineation over the constant threshold is two folds: (1) Ability to capture the seasonal variability that prevents the natural low flow season to be detected under drought (2) enables detections of various drought characteristics rather than instantaneous drought onset and termination points as followed in the standardized index-based drought detection approach (*e.g.*, standardized indices of precipitation[75] and streamflow[76]). For the threshold determination, 366 (an additional day for leap year) flow duration curves are developed using continuous time series of streamflow records. Following the literature[15,16,77,78], an 20th percentile threshold (flow equaled or exceeded 80% of the flow record) is selected for each day of the year forming the variable threshold time series. Since the daily threshold time series appeared to be a jagged curve resulting in several short deficit periods, a centered moving average of 30 days is applied as a smoothing filter[19,22]. A drought episode is detected when the daily streamflow time series falls below the variable threshold.

After identifying drought events, next, we further categorize streamflow-based droughts into several characteristics[19,79] (see **Fig. 1b**). Drought duration is the period in which streamflow is lower than the threshold continuously for 30 days or more (this phase is shown from t_{sp} to t_{ep} in **Fig. 1b**, where '*s*' denotes initiation, '*e*' is the termination point and '*p*' indicates persistence phase). Following Ahmadi and Moradkhani (2018)[19], we select the threshold time window of 30 days based on the consideration of the natural variation and long enough to filter out the inter-seasonal anomalies. Following the refs.[19,20,79] we detect the drought growth as moving 60 days back from the drought termination, when the streamflow falls above the threshold for less than 15 days, *i.e.*, the occurrence of short deficits interrupted by less than 15 days of above-normal streamflow (in **Fig. 1b**: t_{sg} to t_{eg}, where 's' is the initiation, 'e' is the termination, and 'g' denotes the growth). We detect the recovery period as moving 60 days forward from the end of the persistence phase, when the streamflow falls below the threshold for less than 15 days (in **Fig. 1b**: t_{sr} to t_{er} where 's' is the initiation, 'e' denotes the termination and '*r*' shows the recovery phase). If the streamflow time series persistently remains below the threshold for more than 15 days then we mark 'no recovery' and the following episode is then considered as a part of a multi-season drought event. Finally, we quantify DTR as the magnitude of change in flow from the Maximum Drought Deficit volume (MDD, the day with the largest negative departure from normal streamflow between the time of the start of drought development and the time of the end of drought termination in **Fig. 1b** - for details please see last but one paragraph in page 4267 in Parry et al[79]) to the peak surplus flow (PS, **Fig. 1b**), divided by the time taken for this transition.

We determine the seasonality in drought termination using directional (or circular) statistics. The termination date is used as a directional variable[31] (**SI 1.1**), in which the position of the mean termination date can be determined using angles (Eq. 1.3 in **SI 1.1**). Following the ref.[80], we calculate the mean termination day (i.e., mean direction of the day of drought termination as described by the circular data) and its variance by weighing the deficit volume (see **SI 1.1**), ensuring the events are given importance as per the persistency of the event.

Digital Soil Mapping (DSM)

We develop Digital soil maps primarily for nine different soil parameters, *e.g.*, sand and clay contents; SOC contents, SOC stock; pH; CEC; moisture contents at field capacity and permanent wilting point; and available water capacity for the Indian subcontinent at six standard depths (0-5, 5-15, 15-30, 30-60, 60-100, and 100-200 cm respectively) according to the GlobalSoilMap specifications[81]. We develop DSMs using an Indian soil legacy database that utilized archived data from various sources, such as the National Bureau of Soil Survey and Land Use Planning (NBSS&LUP) and other institution publications[18]. The newly developed, digital soil map follows *scorpan* model[82], in which a soil property at an unknown location is estimated as a function of environmental covariates. The environmental covariates used in generating the current maps include terrain attributes derived from the 90 m shuttle radar topographic mission (SRTM) digital elevation model (DEM) data[83] and climate covariates, which includes mean monthly temperature and precipitation[18].Soil parameters (**Table S1**) for top 30 (weighted average of depths 0-5, 5-15, 15-30 cm) and 100 cm (weighted average of depths 0-5, 5-15, 15-30, 30-60, 60-100 cm) soil layers are extracted over the selected catchments of PRB.

Linking Drought Stages with Climate-Catchment-Soil Controls

To identify the potential KDDs in influencing drought dynamics, first we perform a non-parametric correlation analysis. Table S1 lists all 89 covariates that are chosen to identify key drought drivers (KDD). Among climatological attributes, we also consider several hydro-meteorological indices, especially for extremes calculated from monthly time series of precipitation (Rainfall_20p), temperature (TX90p), PET (PETX_20p), and soil moisture (SMX_20p), which are widely used for analysing climatic extremes at the regional and global scales[84,85]. These extreme indices are calculated by calculating the median of the values greater (or lower) than equal to the n^{th} percentile (where, $n = 20$ for deficit and 90 for surplus as adopted here) of each meteorological variable. Next, we perform dependency analysis between each KDD and catchment-wise median drought stages using Kendall's τ, which is robust to the small number of outliers (unlike Pearson's correlation coefficient) and discrepancies in the data[86]. We check the statistical significance of dependence at 10% significance level with p-value < 0.1.

Finally, to select KDDs influencing the drought stages, we implement a hybrid feature selection procedure consisting of filtering and wrapping through Boruta algorithm[53], which is built around the random forest classification algorithm. For filtering, we retain the covariates exhibiting significant (p-value < 0.1) association with drought stages in the Kendall's rank correlation. Subsequently, we apply Boruta on the reduced set of significant variables to obtain the key drought drivers (KDDs) by fixing the number of iterations as 1000 (**Fig. 1c**). This was achieved by creating 'shadow' attributes for each original attribute from shuffling the corresponding values of original covariates across stations. Finally, we perform feature selection by using the random forest classification algorithm and compute the importance of all attributes of this extended system with reference to maximum Z-score of shadow attributes (MZSA). We mark the variables significant when they have ‘importance’[53] significantly higher than that of MZSA and discard the variables that show ‘importance’ lower than that of MZSA.

Data Availability

All the data used in this study are publicly available. The precipitation data is obtained from Global Precipitation Climatology Centre (https://opendata.dwd.de/climate_environment/GPCC/html/fulldata_v7_doi_download.html). The monthly soil moisture data is obtained from the Climate Prediction Center (CPC; https://psl.noaa.gov/data/gridded/data.cpcsoil.html). The monthly mean surface air temperature is obtained from the CPC Global land surface air temperature data (https://ual.geoplatform.gov/api/items/ff4f9af65d322c28a421cf569471d216.html). The PET time series is obtained from the Climate Research Unit’s (CRU) version 4.04 database (https://crudata.uea.ac.uk/cru/data/hrg/). All data are available at a 0.5° spatial resolution in a monthly time scale. The shapefiles for the Indian river basins are obtained from the Global Streamflow Indices and Metadata Archive (https://doi.pangaea.de/10.1594/PANGAEA.887477). The digital elevation map to develop terrain features are derived from the 90 m SRTM DEM database (https://cgiarcsi.community/data/srtm-90m-digital-elevation-database-v4-1/). The digital soil mapping for India was developed using an Indian soil legacy database that utilized archived data from various sources, such as the National Bureau of Soil Survey and Land Use Planning (NBSS&LUP; https://www.nbsslup.in/) and other institution publications[18].

Code Availability

The MATLAB Codes used for drought characteristics and delineation of drought regimes have been archived by the authors and are available on request from P.G., pganguli@agfe.iitkgp.ac.in. The source codes for Digital Soil Map of India codes are available from authors through personal request.

Acknowledgment

PG is supported through Science and Engineering Research Board, Government of India’s early career start-up grant, SRG/2019/000044.

Contributions

PG contributed to overall concept development, writing, prepared initial data processing scripts in MATLAB for hydrological droughts and final edits; BJS and AR performed data collection and screening of the time series; BJS performed drought data analysis and prepared the first draft; NNR performed digital soil mapping and prepared corresponding write-up; AR analyzed rainfall data and land-use pattern and contributed to writing; DM carried out feature selection analyses and performed the data interpretation with the help of BSD and PG and wrote feature selection part; BSD conceived soil control concept and performed final edits. All co-authors discussed the results, reviewed and approved the final manuscript.

Competing Interests

The authors declare no competing interests.

References

1. NASA earth observatory. Water Shortages in India. https://earthobservatory.nasa.gov/images/145242/water-shortages-in-india (2019).
2. Ghosh, S. & Srinivasan, K. Analysis of Spatio-temporal Characteristics and Regional Frequency of Droughts in the Southern Peninsula of India. *Water Resour Manage* **30**, 3879–3898 (2016).
3. Bisht, D. S., Sridhar, V., Mishra, A., Chatterjee, C. & Raghuwanshi, N. S. Drought characterization over India under projected climate scenario. *International Journal of Climatology* **39**, 1889–1911 (2019).
4. Nations, U. World population prospects 2019: highlights. *Department of Economic and Social Affairs, Population Division* (2019).
5. Parvatam, S. & Priyadarshini, S. On Day Zero, India prepares for a water emergency. *Nature India* https://www.natureasia.com/en/nindia/article/10.1038/nindia.2019.84 (2019).
6. Flatau, M. K., Flatau, P. J., Schmidt, J. & Kiladis, G. N. Delayed onset of the 2002 Indian monsoon. *Geophysical research letters* **30**, (2003).
7. Schewe, J. & Levermann, A. A statistically predictive model for future monsoon failure in India. *Environmental Research Letters* **7**, 044023 (2012).
8. Mishra, V., Thirumalai, K., Jain, S. & Aadhar, S. Unprecedented drought in South India and recent water scarcity. *Environ. Res. Lett.* (2021) doi:10.1088/1748-9326/abf289.
9. Dracup, J. A., Lee, K. S. & Paulson Jr, E. G. On the definition of droughts. *Water resources research* **16**, 297–302 (1980).
10. Shah, D. & Mishra, V. Drought Onset and Termination in India. *Journal of Geophysical Research: Atmospheres* **125**, e2020JD032871 (2020).
11. Bhardwaj, K., Shah, D., Aadhar, S. & Mishra, V. Propagation of Meteorological to Hydrological Droughts in India. *Journal of Geophysical Research: Atmospheres* **125**, e2020JD033455 (2020).
12. Van Loon, A. F., Van Huijgevoort, M. H. J. & Van Lanen, H. a. J. Evaluation of drought propagation in an ensemble mean of large-scale hydrological models. *Hydrology and Earth System Sciences* **16**, 4057–4078 (2012).
13. Gevaert, A., Veldkamp, T. & Ward, P. The effect of climate type on timescales of drought propagation in an ensemble of global hydrological models. *Hydrology and Earth System Sciences* **22**, 4649–4665 (2018).
14. Van Loon, A. F. *et al.* How climate seasonality modifies drought duration and deficit. *Journal of Geophysical Research: Atmospheres* **119**, 4640–4656 (2014).
15. Van Loon, A. F. Hydrological drought explained. *Wiley Interdisciplinary Reviews: Water* **2**, 359–392 (2015).
16. Van Loon, A. F. & Laaha, G. Hydrological drought severity explained by climate and catchment characteristics. *Journal of Hydrology* **526**, 3–14 (2015).
17. Van Lanen, H. A., Wanders, N., Tallaksen, L. M. & Van Loon, A. F. Hydrological drought across the world: impact of climate and physical catchment structure. *Hydrology and Earth System Sciences* **17**, 1715–1732 (2013).
18. Reddy, N. N. *et al.* Legacy data-based national-scale digital mapping of key soil properties in India. *Geoderma* **381**, 114684 (2021).

19. Ahmadi, B. & Moradkhani, H. Revisiting hydrological drought propagation and recovery considering water quantity and quality. *Hydrological Processes* **33**, 1492–1505 (2019).
20. Ahmadi, B., Ahmadalipour, A. & Moradkhani, H. Hydrological drought persistence and recovery over the CONUS: A multi-stage framework considering water quantity and quality. *Water research* **150**, 97–110 (2019).
21. Bonnafous, L. & Lall, U. Space-time clustering of climate extremes amplify global climate impacts, leading to fat-tailed risk. *Natural Hazards and Earth System Sciences Discussions* 1–19 (2020) doi:10.5194/nhess-2019-405.
22. Heudorfer, B. & Stahl, K. Comparison of different threshold level methods for drought propagation analysis in Germany. *Hydrology Research* **48**, 1311–1326 (2017).
23. Schneider, U. *et al.* GPCC full data reanalysis version 6.0 at 0.5: Monthly land-surface precipitation from rain-gauges built on GTS-based and historic data. *GPCC Data Rep., doi* **10**, (2011).
24. Fan, Y. & Van den Dool, H. A global monthly land surface air temperature analysis for 1948–present. *Journal of Geophysical Research: Atmospheres* **113**, (2008).
25. Harris, I., Osborn, T. J., Jones, P. & Lister, D. Version 4 of the CRU TS monthly high-resolution gridded multivariate climate dataset. *Scientific data* **7**, 1–18 (2020).
26. Van den Dool, H., Huang, J. & Fan, Y. Performance and analysis of the constructed analogue method applied to US soil moisture over 1981–2001. *Journal of Geophysical Research: Atmospheres* **108**, (2003).
27. Do, H. X., Gudmundsson, L., Leonard, M. & Westra, S. The Global Streamflow Indices and Metadata Archive (GSIM) – Part 1: The production of a daily streamflow archive and metadata. *Earth System Science Data* **10**, 765–785 (2018).
28. Minasny, B. *et al.* Soil carbon 4 per mille. *Geoderma* **292**, 59–86 (2017).
29. Sahana, V., Sreekumar, P., Mondal, A. & Rajsekhar, D. On the rarity of the 2015 drought in India: A country-wide drought atlas using the multivariate standardized drought index and copula-based severity-duration-frequency curves. *Journal of Hydrology: Regional Studies* **31**, 100727 (2020).
30. IOH (Institute of Hydrology). Low Flow Studies Report no.1 Research Report. *NERC Open Research Archive* http://nora.nerc.ac.uk/id/eprint/9093/1/Low_Flow_01.pdf (1980).
31. Mardia, K. V. Statistics of directional data. *Journal of the Royal Statistical Society: Series B (Methodological)* **37**, 349–371 (1975).
32. Burn, D. H. & Arnell, N. W. Synchronicity in global flood responses. *Journal of Hydrology* **144**, 381–404 (1993).
33. Bhat, G. S. The Indian drought of 2002—a sub-seasonal phenomenon? *Quarterly Journal of the Royal Meteorological Society* **132**, 2583–2602 (2006).
34. Bezdek, J. C. A convergence theorem for the fuzzy ISODATA clustering algorithms. *IEEE transactions on pattern analysis and machine intelligence* 1–8 (1980).
35. Ross, T. J. *Fuzzy logic with engineering applications*. (John Wiley & Sons, 2005).
36. Burn, D. H. Catchment similarity for regional flood frequency analysis using seasonality measures. *Journal of hydrology* **202**, 212–230 (1997).
37. Mujumdar, P. & Ghosh, S. Modeling GCM and scenario uncertainty using a possibilistic approach: Application to the Mahanadi River, India. *Water Resources Research* **44**, (2008).

38. Naveena, N., Satyanarayana, G. Ch., Rao, D. V. B. & Srinivas, D. An accentuated "hot blob" over Vidarbha, India, during the pre-monsoon season. *Nat Hazards* **105**, 1359–1373 (2021).
39. Rumsey, C. A., Miller, M. P., Susong, D. D., Tillman, F. D. & Anning, D. W. Regional scale estimates of baseflow and factors influencing baseflow in the Upper Colorado River Basin. *Journal of Hydrology: Regional Studies* **4**, 91–107 (2015).
40. Laaha, G. & Blöschl, G. Seasonality indices for regionalizing low flows. *Hydrological Processes: An International Journal* **20**, 3851–3878 (2006).
41. Bhagat, H., Ghosh, P. & Nagesh Kumar, D. Estimation of seasonal base flow contribution to a tropical river using stable isotope analysis. *Journal of Hydrology* **601**, 126661 (2021).
42. Beck, H. E. *et al.* Global patterns in base flow index and recession based on streamflow observations from 3394 catchments. *Water Resources Research* **49**, 7843–7863 (2013).
43. Samra, J. S. *Review and analysis of drought monitoring, declaration and management in India*. vol. 84 (IWMI, 2004).
44. Mujumdar, M. *et al.* Droughts and Floods. in *Assessment of Climate Change over the Indian Region: A Report of the Ministry of Earth Sciences (MoES), Government of India* (eds. Krishnan, R. et al.) 117–141 (Springer, 2020). doi:10.1007/978-981-15-4327-2_6.
45. Parry, S., Prudhomme, C., Wilby, R. L. & Wood, P. J. Drought termination: Concept and characterisation. *Progress in Physical Geography* **40**, 743–767 (2016).
46. Kelly, L. *et al.* Quantification of temporal variations in base flow index using sporadic river data: application to the Bua catchment, Malawi. *Water* **11**, 901 (2019).
47. Tallaksen, L. M. & Van Lanen, H. A. Hydrological drought: processes and estimation methods for streamflow and groundwater. (2004).
48. Bloomfield, J. P., Allen, D. J. & Griffiths, K. J. Examining geological controls on baseflow index (BFI) using regression analysis: An illustration from the Thames Basin, UK. *Journal of Hydrology* **373**, 164–176 (2009).
49. Salinas, J. L. *et al.* Comparative assessment of predictions in ungauged basins–Part 2: Flood and low flow studies. *Hydrology and Earth System Sciences* **17**, 2637–2652 (2013).
50. Beven, K. J. & Kirkby, M. J. A physically based, variable contributing area model of basin hydrology/Un modèle à base physique de zone d'appel variable de l'hydrologie du bassin versant. *Hydrological Sciences Journal* **24**, 43–69 (1979).
51. Beven, K. J., Kirkby, M. J., Freer, J. E. & Lamb, R. A history of TOPMODEL. *Hydrology and Earth System Sciences* **25**, 527–549 (2021).
52. Yaeger *et al.* Exploring the physical controls of regional patterns of flow duration curves – Part 4: A synthesis of empirical analysis, process modeling and catchment classification. *Hydrology and Earth System Sciences* **16**, 4483–4498 (2012).
53. Kursa, M. B. & Rudnicki, W. R. Feature selection with the Boruta package. *J Stat Softw* **36**, 1–13 (2010).
54. Yang, Y. *et al.* Lags in hydrologic recovery following an extreme drought: Assessing the roles of climate and catchment characteristics. *Water Resources Research* **53**, 4821–4837 (2017).
55. Zhou, S. *et al.* Land–atmosphere feedbacks exacerbate concurrent soil drought and atmospheric aridity. *PNAS* **116**, 18848–18853 (2019).

56. Brunner, M. I., Swain, D. L., Gilleland, E. & Wood, A. W. Increasing importance of temperature as a contributor to the spatial extent of streamflow drought. *Environ. Res. Lett.* **16**, 024038 (2021).
57. Iizumi, T. & Wagai, R. Leveraging drought risk reduction for sustainable food, soil and climate via soil organic carbon sequestration. *Scientific reports* **9**, 1–8 (2019).
58. Loon, A. F. V. *et al.* How climate seasonality modifies drought duration and deficit. *Journal of Geophysical Research: Atmospheres* **119**, 4640–4656 (2014).
59. Singh, A., Reager, J. T. & Behrangi, A. Estimation of hydrological drought recovery based on precipitation and Gravity Recovery and Climate Experiment (GRACE) water storage deficit. *Hydrology and Earth System Sciences* **25**, 511–526 (2021).
60. Wlostowski, A. N. *et al.* Signatures of hydrologic function across the Critical Zone Observatory network. *Water Resources Research* **57**, e2019WR026635 (2021).
61. Ukkola, A. M. *et al.* Land surface models systematically overestimate the intensity, duration and magnitude of seasonal-scale evaporative droughts. *Environ. Res. Lett.* **11**, 104012 (2016).
62. Zhou, Y. *et al.* Developing a hydrological monitoring and sub-seasonal to seasonal forecasting system for South and Southeast Asian river basins. *Hydrology and Earth System Sciences* **25**, 41–61 (2021).
63. Esit, M. *et al.* Seasonal to multi-year soil moisture drought forecasting. *npj Clim Atmos Sci* **4**, 1–8 (2021).
64. Shah, R. D. & Mishra, V. Development of an Experimental Near-Real-Time Drought Monitor for India. *Journal of Hydrometeorology* **16**, 327–345 (2015).
65. Sutanto, S. J., Wetterhall, F. & Lanen, H. A. J. V. Hydrological drought forecasts outperform meteorological drought forecasts. *Environ. Res. Lett.* **15**, 084010 (2020).
66. Portele, T. C. *et al.* Seasonal forecasts offer economic benefit for hydrological decision making in semi-arid regions. *Sci Rep* **11**, 10581 (2021).
67. AghaKouchak, A. *et al.* Climate Extremes and Compound Hazards in a Warming World. *Annu. Rev. Earth Planet. Sci.* **48**, 519–548 (2020).
68. Anderegg, W. R. L. *et al.* Pervasive drought legacies in forest ecosystems and their implications for carbon cycle models. *Science* **349**, 528–532 (2015).
69. Lal, R. Soil Carbon Sequestration Impacts on Global Climate Change and Food Security. *Science* (2004) doi:10.1126/science.1097396.
70. Oelkers, E. H. & Cole, D. R. Carbon Dioxide Sequestration A Solution to a Global Problem. *Elements* **4**, 305–310 (2008).
71. Ministry of Agriculture. *Land Use Statistics at a Glance from 2007–08 to 2016–17*. https://eands.dacnet.nic.in/LUS_1999_2004.htm (2021).
72. Ganguli, P. & Ganguly, A. R. Space-time trends in U.S. meteorological droughts. *Journal of Hydrology: Regional Studies* **8**, 235–259 (2016).
73. Ganguli, P., Nandamuri, Y. R. & Chatterjee, C. Analysis of persistence in the flood timing and the role of catchment wetness on flood generation in a large river basin in India. *Theor Appl Climatol* (2019) doi:10.1007/s00704-019-02964-z.
74. Gustard, A. & Demuth, S. *Manual on low-flow estimation and prediction*. (Opera, 2009).
75. McKee, T. B., Doesken, N. J. & Kleist, J. The relationship of drought frequency and duration to time scales. in *Proceedings of the 8th Conference on Applied Climatology* vol. 17 179–183 (Boston, 1993).

76. Shukla, S. & Wood, A. W. Use of a standardized runoff index for characterizing hydrologic drought. *Geophysical Research Letters* **35**, (2008).
77. Parry, S., Hannaford, J., Lloyd-Hughes, B. & Prudhomme, C. Multi-year droughts in Europe: analysis of development and causes. *Hydrology Research* **43**, 689–706 (2012).
78. Sutanto, S. J. & Van Lanen, H. A. J. Streamflow drought: implication of drought definitions and its application for drought forecasting. *Hydrology and Earth System Sciences* **25**, 3991–4023 (2021).
79. Parry, S., Wilby, R. L., Prudhomme, C. & Wood, P. J. A systematic assessment of drought termination in the United Kingdom. *Hydrology and Earth System Sciences* **20**, 4265–4281 (2016).
80. Burn, D. H. & Whitfield, P. H. Changes in flood events inferred from centennial length streamflow data records. *Advances in Water Resources* **121**, 333–349 (2018).
81. Arrouays, D., McKenzie, N., Hempel, J., de Forges, A. R. & McBratney, A. B. *GlobalSoilMap: basis of the global spatial soil information system*. (CRC press, 2014).
82. McBratney, A. B., Santos, M. M. & Minasny, B. On digital soil mapping. *Geoderma* **117**, 3–52 (2003).
83. Jarvis, A., Guevara, E., Reuter, H. I. & Nelson, A. D. Hole-filled SRTM for the globe: version 4: data grid. (2008).
84. Alexander, L. V. *et al.* Intercomparison of annual precipitation indices and extremes over global land areas from in situ, space-based and reanalysis products. *Environ. Res. Lett.* **15**, 055002 (2020).
85. Klein Tank, A. M. G., Zwiers, F. W. & Zhang, X. Guidelines on analysis of extremes in a changing climate in support of informed decisions for adaptation. WCDMP-72. *World Meteorological Organization, Geneva, Switzerland* (2009).
86. Chok, N. S. Pearson's versus Spearman's and Kendall's correlation coefficients for continuous data. (University of Pittsburgh, 2010).

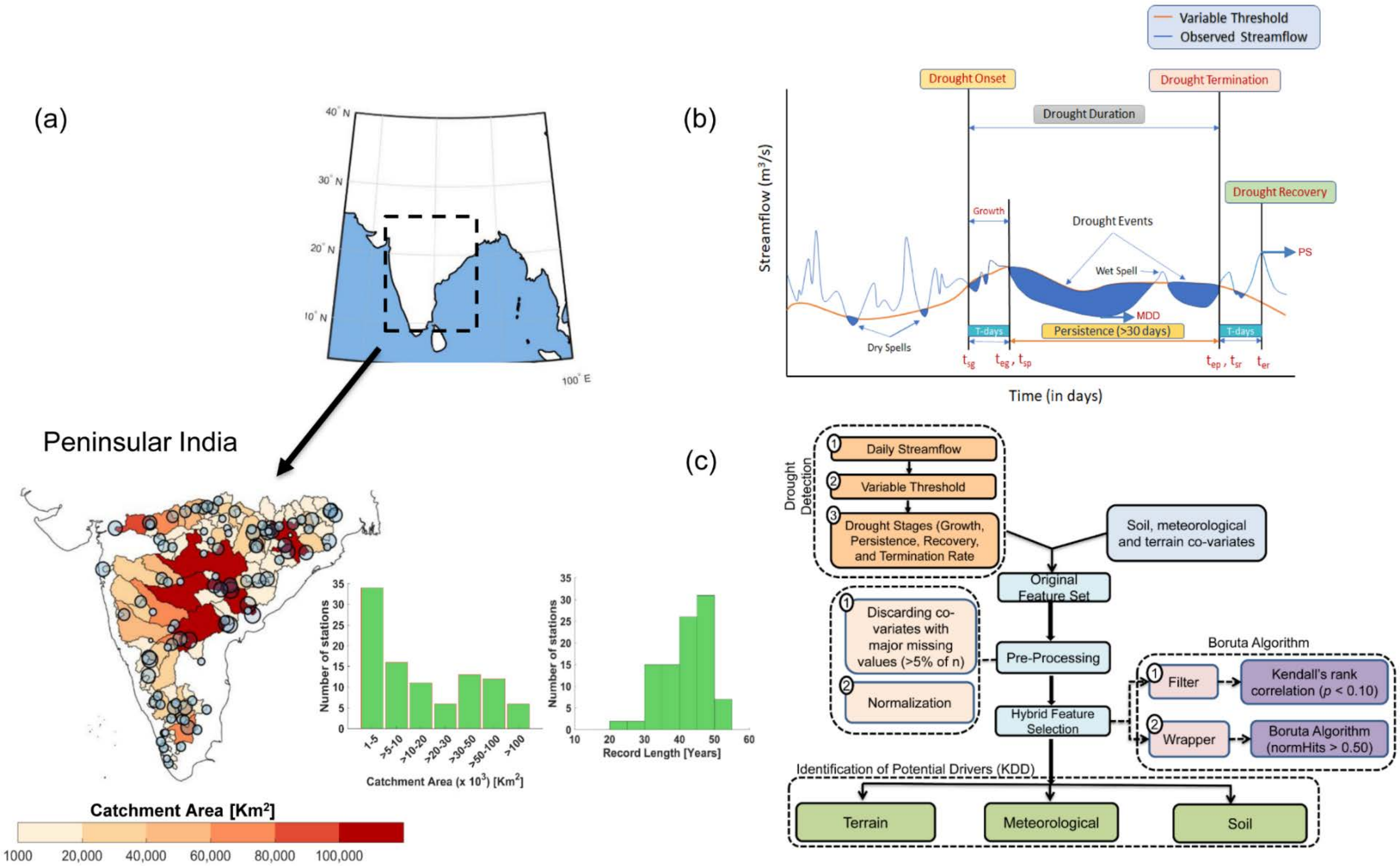

Fig. 1 Distribution of stream gauges, drought characteristics and conceptual diagram illustrating KDD detection. (a) Location of stream gauges within each catchment. The size of bubbles shows the record length which is proportional to the sample length (in years). Histograms show the distribution of catchment area (in km^2), and available record lengths (in years). **(b)** Identification of drought characteristics using daily variable threshold approach. The blue shaded region depicts streamflow deficit. The t_{sg} and t_{eg} represent the start and end of the growth period. Likewise, t_{sp} and t_{ep} indicate the initiation and termination of the drought persistence stage. t_{sr} and t_{er} denote the initiation and termination of the drought recovery, MDD and PS indicate maximum drought deficit volume during the persistence stage and peak surplus flow after drought termination. **(C)** Detection of Key Drought Drivers (KDD's) using random forest-based feature selection algorithm. The threshold criterion, normHits > 0.50 indicates only those features are selected that show higher 'importance' than their shadow attributes (obtained by random permutation of features) for more than 50% of total iterations.

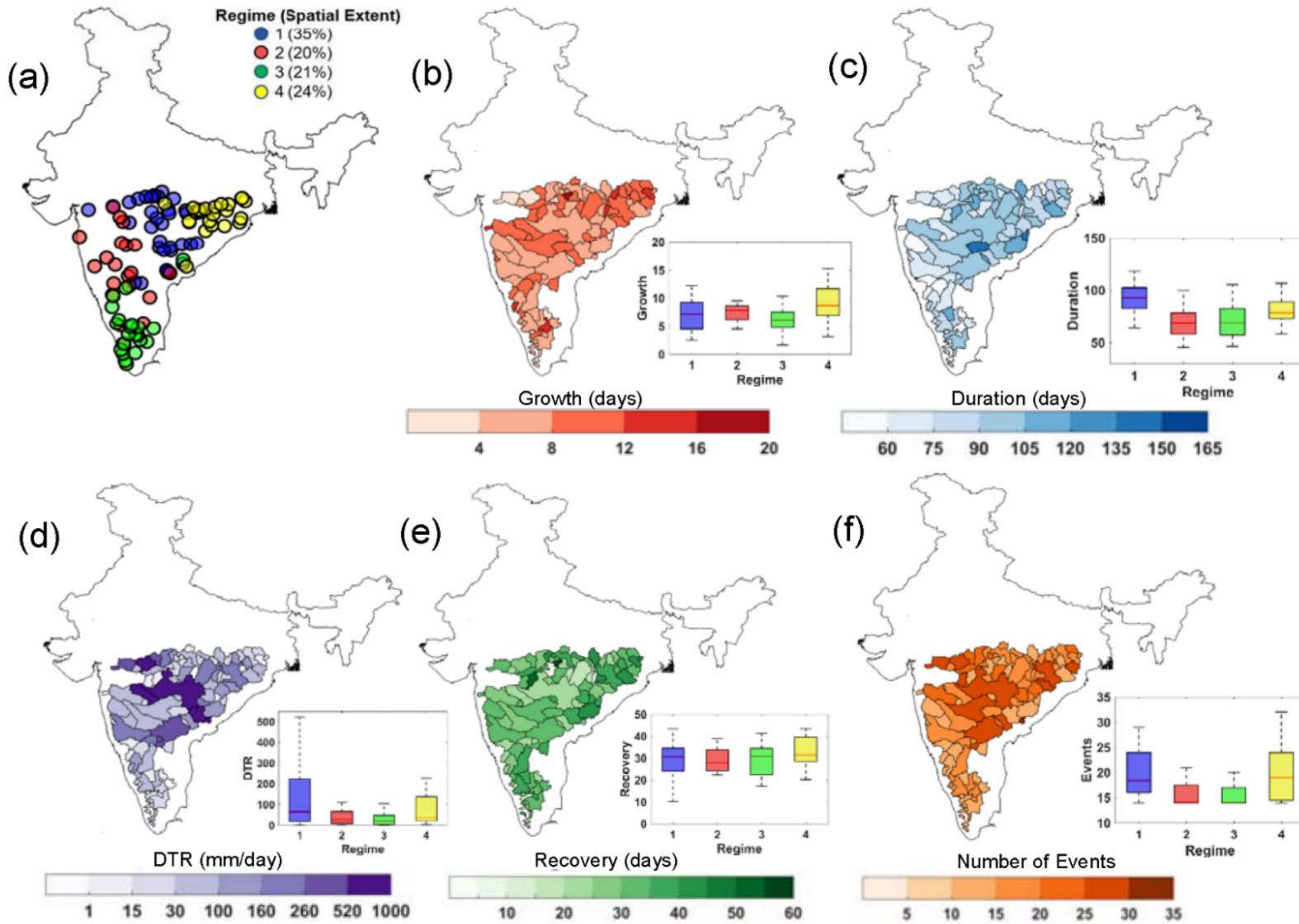

Fig. 2 Identification of drought regimes and illustration of Catchment-scale Drought Properties. (a) Regionalization of droughts based on drought characteristics using fuzzy c means clustering algorithm (see Methods); *n* indicates the number of sites detected within each cluster. **(b – f)** Spatial distributions of drought characteristics during 1965-2018 time window: **(b)** drought growth (in days) **(c)** duration (days) **(d)** drought termination rate or DTR (mm/day) (**e**) recovery period (in days) **(f)** drought frequency or number of events. The boxplots in inset show the variability in drought properties among the identified clusters. Box center marks (red lines) are medians; box bottom and top edges show 25th and 75th percentiles respectively, whereas the spread of the boxes indicates interquartile range; whiskers indicate q75 + 1.5(q75 – q25) and q25 - 1.5(q75 – q25), where q is the quantiles of variables. The shades of boxes in purple, red, green and yellow indicate streamflow drought regimes 1 – 4, based on selected drought attributes.

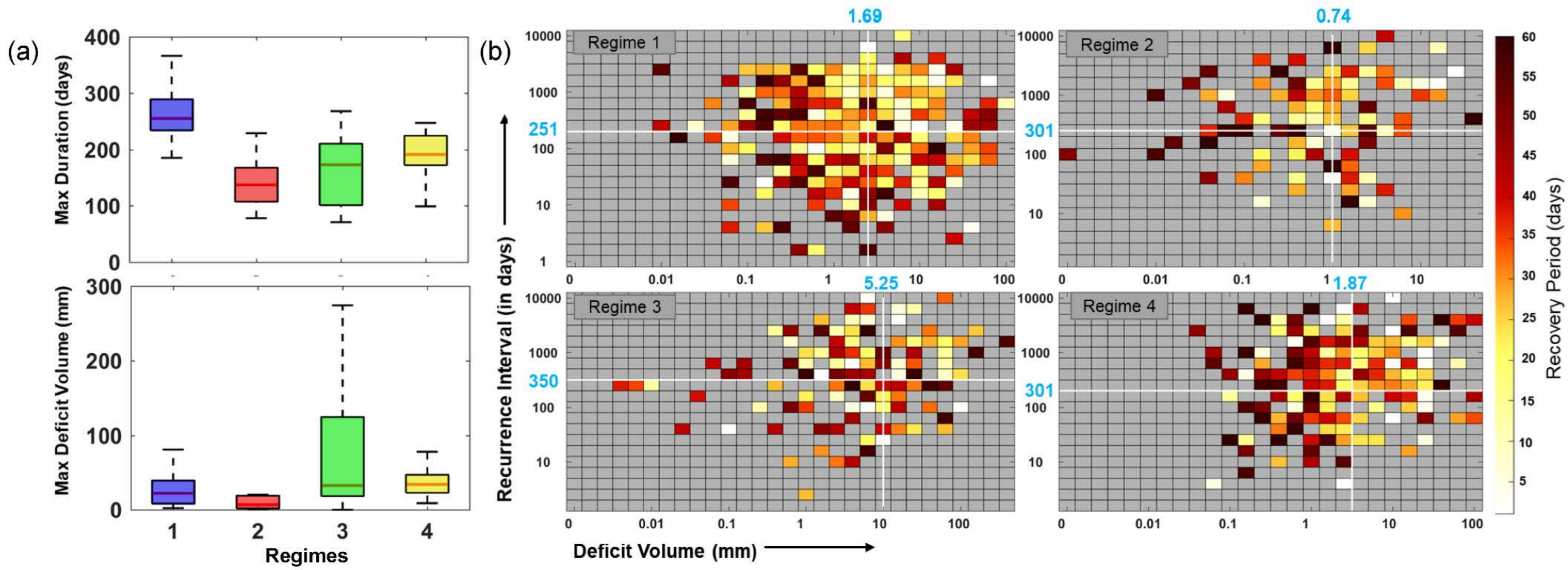

Fig. 3 Variations in drought properties, maximum severity, maximum duration, and recovery times among the detected clusters. (a) The boxplots showing interquartile range of selected drought attributes, the (maximum) duration and the deficit volume. **(b)**The recovery period as a function of deficit volume and recurrence interval (*i.e.*, the time interval between two successive droughts but neglecting the first drought event) for the identified regimes. The shades of each pixel show the drought recovery period. The cells in grey indicates no observation. The straight lines in white perpendicular to the axes show the median deficit volume and the median recurrence interval for each region.

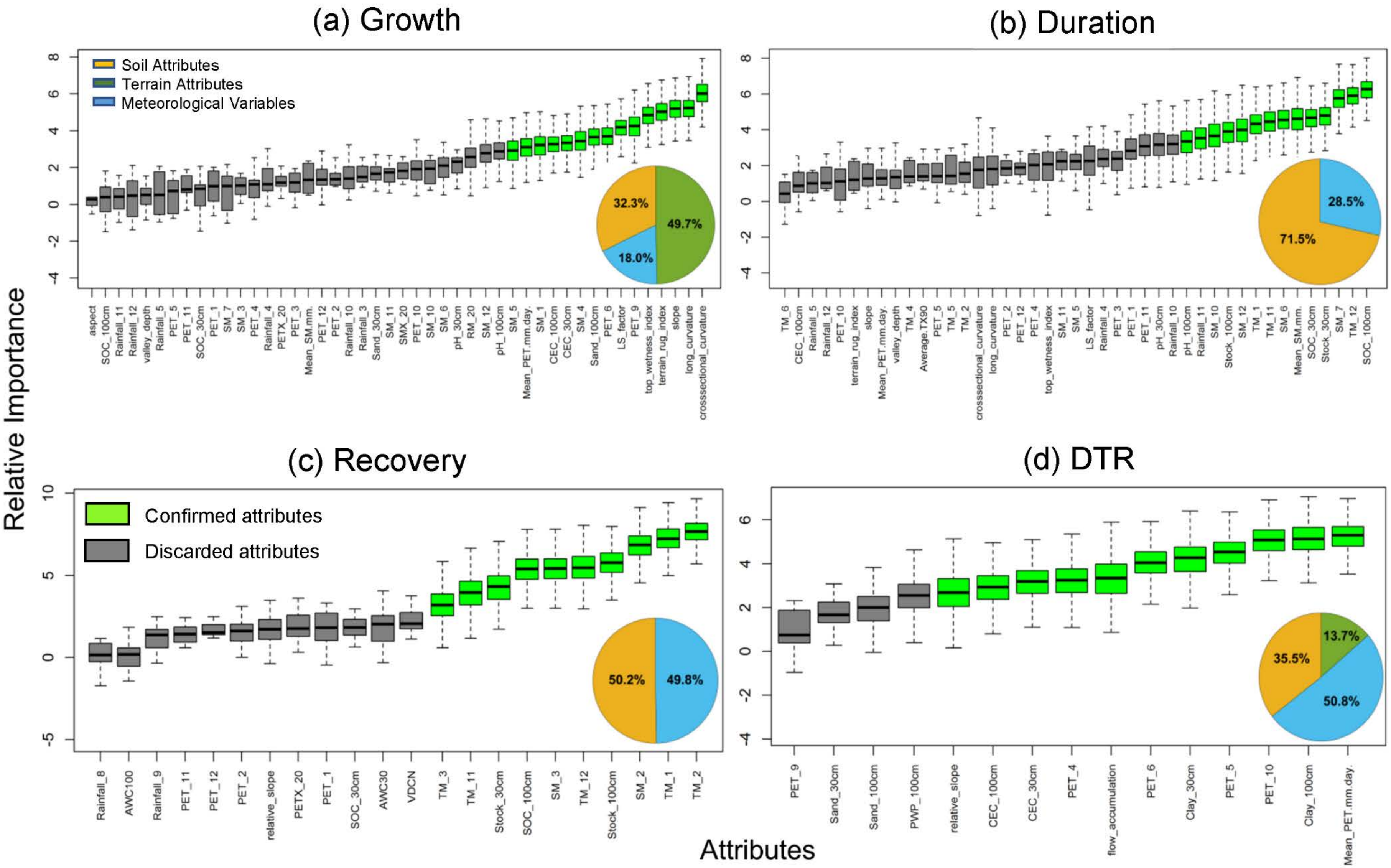

Fig. 4 Potential Key Drought Drivers. The relative importance of key drought drivers is shown using box plots for various drought characteristics. The pie charts at the lower bottom corner show relative contribution of soil, terrain and meteorological variables in influencing drought stages. The x-axes show the soil-climate and topographical attributes; details of each of these attributes are described in **Table S1**. The legends applies to all figure panels.

Supplementary Information for

Climate-Catchment-Soil Control on Hydrological Droughts in Peninsular India

Poulomi Ganguli[1,*,#], Bhupinderjeet Singh[1,#], Nagarjuna N. Reddy[1], Aparna Raut[1], Debasish Mishra[1], Bhabani Sankar Das[1]

[1]Agricultural and Food Engineering Department, Indian Institute of Technology Kharagpur, West Bengal, Kharagpur 721302, India

[*]Corresponding Author: pganguli@agfe.iitkgp.ac.in

[#]These authors contributed equally to this work.

SI. 1.1 Determination of Seasonality in Drought Termination

The termination date of each drought event is plotted on the circle with unit radius, where the position of the event is defined by θ_i

$$\theta_i = \frac{2\pi * D}{T} \tag{1.1}$$

where T is the number of days in the year, D is the termination date which varies from 1 to 365 days in a non-leap year (366 days in a leap year), The position of the mean termination date can be determined using the angles, converting it to x and y coordinates:

$$\bar{x} = \frac{\sum_{i=1}^{n} q_i \cos \theta i}{\sum_{i=1}^{n} q_i} \qquad \bar{y} = \frac{\sum_{i=1}^{n} q_i \sin \theta i}{\sum_{i=1}^{n} q_i} \tag{1.2}$$

where q_i = Deficit volume for the event 'i'

The mean direction of the circular Data ($\bar{\eta}$) is determined as:

$$\bar{\eta} = \begin{cases} \tan^{-1}\left(\dfrac{\bar{y}}{\bar{x}}\right) & if\ \bar{x} > 0\ and\ \bar{y} > 0 \\ 180 - \tan^{-1}\left(\dfrac{\bar{y}}{\bar{x}}\right) & if\ \bar{x} < 0\ and\ \bar{y} > 0 \\ 180 + \tan^{-1}\left(\dfrac{\bar{y}}{\bar{x}}\right) & if\ \bar{x} < 0\ and\ \bar{y} < 0 \\ 360 + \tan^{-1}\left(\dfrac{\bar{y}}{\bar{x}}\right) & if\ \bar{x} > 0\ and\ \bar{y} < 0 \\ \pi/2 & if\ \bar{x} = 0\ and\ \bar{y} > 0 \\ 3\pi/2 & if\ \bar{x} = 0\ and\ \bar{y} < 0 \end{cases} \tag{1.3}$$

Mean Event Date can be calculated as: $\omega = \tan^{-1}(\bar{\eta})\left(\dfrac{len\,\bar{y}}{2\pi}\right)$

Where ω is the mean date of occurrence of the extreme events and $\bar{\eta}$ is computed using Eq. 1.3. $len\,\bar{y}$ indicates the average length of days in a year, considering the number of leap and non-leap days. Finally, to measure the variability in the termination month about mean date is calculated by defining the regularity, $\bar{\phi}$:

$$\bar{\phi} = \sqrt{\bar{x}^2 + \bar{y}^2} \qquad 0 \le \bar{r} \le 1 \tag{1.4}$$

Where, $\bar{\phi}$ = 0 if all the events are terminating uniformly throughout the year (low regularity) and $\bar{\phi}$ =1 if all the events are terminating in the same month (high regularity)

The variability in timing of drought termination is determined using circular variance (s^2):

$$s^2 = -2\ln\left(\bar{\phi}\right) \quad (1.5)$$

SI 1.2 Drought Cluster Identification using Fuzzy Algorithm

Fuzzy C- means (FCM) algorithm was firstly proposed by which was further improved[1,2]. The FCM algorithm assigns the membership to each feature vector with respect to the euclidean distance between the feature vector and cluster center, and it is more generalized and useful to describe a point not by a hard clustering, but by its membership values with respect to all the clusters[3]. The higher the value of fuzzy membership stronger is the relationship of the feature vector with the specific cluster[4]. For a data set of *M* objects and *p* classes, if $\mathbf{X}_k$ is the feature vector of the k^{th} object, where k = 1,2, 3…., *M*, the main aim of the FCM algorithm is to minimize the objective function as defined below:

$$J\,(U, C) = \sum_{j=1}^{M} \sum_{i=1}^{c} u_{ik}^{a}\, \|Y_k - C_i\|^2 \quad (1.6)$$

Where, u_{ik} is the membership value of k^{th} data point in the i^{th} cluster, $\|Y_k - C_i\|^2$ is the Euclidean distance between feature vector k and a center point of i^{th} cluster, C_i is the center value of the i^{th} cluster and α is called as fuzzifier value, which can have any value which is greater than 1. The value closer to 1 provides the cluster solution which is very similar to hard clustering (*e.g.*, K-means clustering) algorithm. In general, fuzzifier value ranges from 1 to 2.5[5].

Fuzzy c-means Algorithm Steps:

1. The number of clusters and the data vector of the cluster center is assumed at random.

2. Membership value matrix is calculated using Eq. (1.6)

$$u_{i<k}^{t+1} = \left[\sum_{j=1}^{c} \left[\frac{\|y_k - c_i\|}{\|y_k - c_j\|}\right]^{\frac{2}{\alpha-1}}\right]^{-1} \quad (1.7)$$

Where i= 1,2,…...c, k=1,2,...,M. j = *1,2.,….c*

3. Using the updated membership values and equation, new values for the cluster center are calculated as below:

$$C_i = \frac{\sum_{k=1}^{M} u_{ik}^{a} y_k}{\sum_{k=1}^{M} u_{ik}^{a}} \quad (1.8)$$

Finally, the clustering process is stopped when it follows a certain stopping criterion. For our case, we stopped the clustering process when two successive iterations reached a value of objective function less than 0.001.

Table S1. List of covariates selected to identify key drought drivers

Attribute types	Specifics of attributes	Abbreviations	Units
Soil	Clay content at 30, 100 cm depth*	Clay_30[1], Clay_100[2]	%
	Sand content at 30, 100 cm depth	sand_30, sand_100	%
	pH at 30, 100 cm depth	pH_30, pH_100	-
	Soil organic content at 30, 100 cm depth	SOC_30, SOC_100	%
	Cation exchange capacity at 30, 100 cm depth	CEC_30, CEC_100	cmol/kg
	Stock at 30, 100 cm depth	Stock	t c/ha
	Field capacity at 30, 100 cm depth	FC	%
	Permanent Wilting Point at 30, 100 cm depth	PWP	%
	Available Water Content at 30 cm, 100 cm depth	AWC	%
	Annual average soil moisture, median monthly soil moisture ≤ 20th percentile threshold	Mean_SM, SMX_20	mm
Climate	Annual average rainfall, mean monthly rainfall from January – December, median monthly rainfall ≤ 20th percentile threshold	Rainfall_*i*, where, *I* = 1, 2,…., 12; RM_20	mm
	Annual average potential evapotranspiration, mean monthly potential evapotranspiration, and median monthly potential evapotranspiration ≤ 20th percentile	Mean_PET, PET_*i* where, *I* = 1, 2,…., 12; PETX_20	mm/day
	Annual average monthly temperature, mean monthly temperature, and median monthly temperature ≥ 90th percentile	TM, TM_*i* where, *I* = 1, 2,…., 12; TX90	mm
Catchment	Aspect		radian
	Channel network base level	CNBL	m
	Convergence Index		-
	Cross-sectional curvature		m^{-1}
	Elevation		m
	Flow accumulation		m^2
	Hill shading		radian
	Longitudinal curvature		m^{-1}
	Slope length-gradient factor	LS-factor	-
	Relative slope position		-
	Slope		radian
	Terrain ruggedness index		-
	Topographic wetness index		-
	Valley depth		m
	Vertical distance to channel network	VDCN	m

*0-30 cm depth indicates the top soil, 30-100 cm indicates the sub-soil; [1] and [2] indicate the 30 cm and 1 m depths respectively.

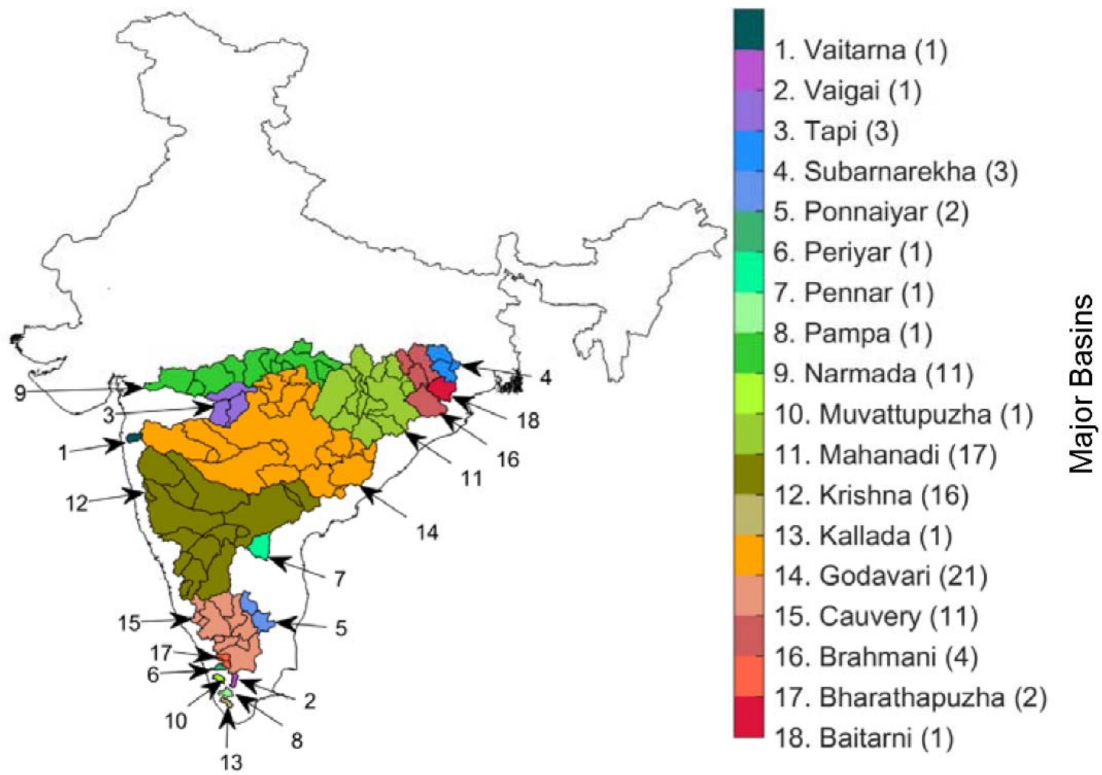

Fig. S1 Locations of large river basins. The numerals in parentheses show the number of sub-catchments within each river basins.

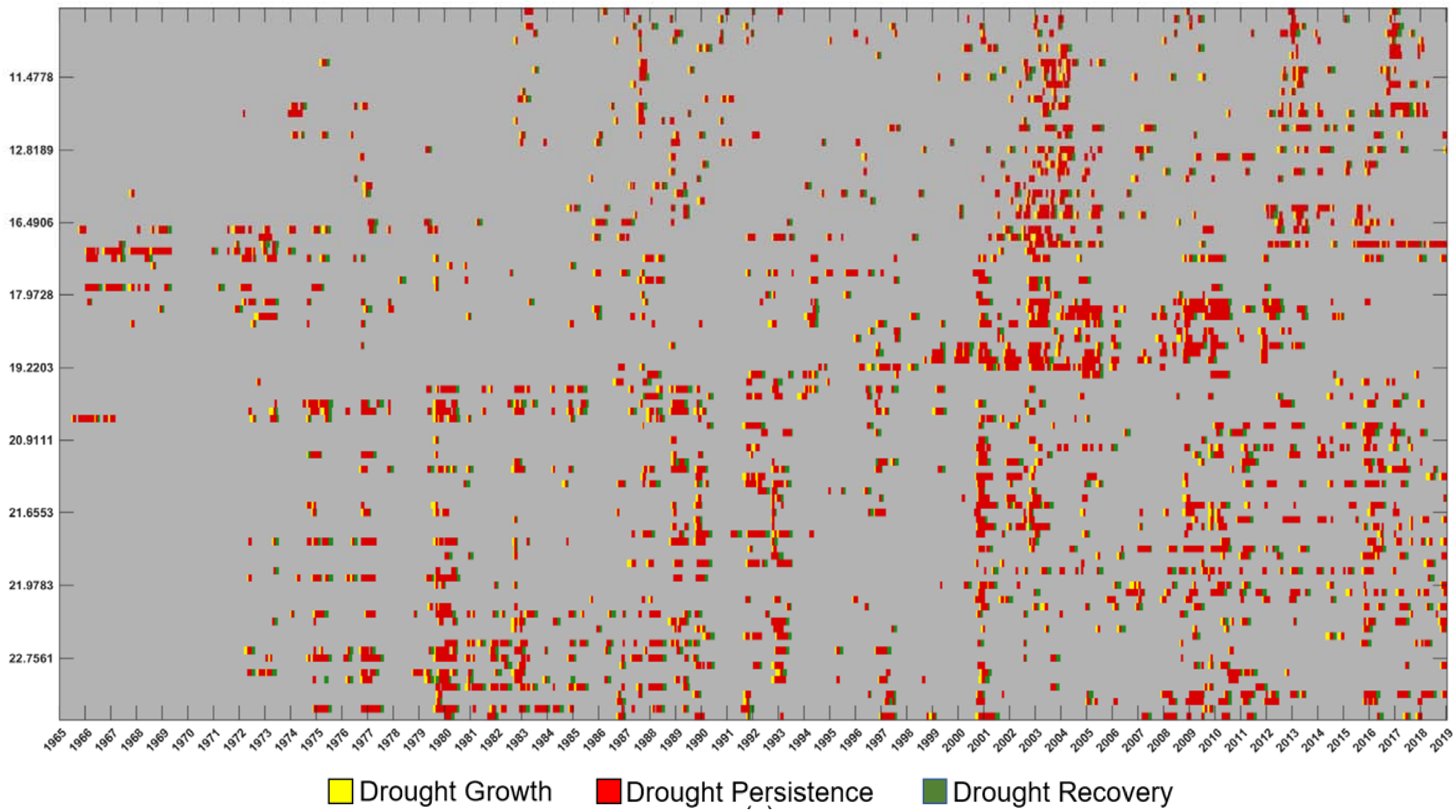

Fig. S2 Hovmöller diagrams (time vs latitude sections) of drought characteristics for the period between 1965 and 2019 over the 98 Peninsular Indian Catchments.

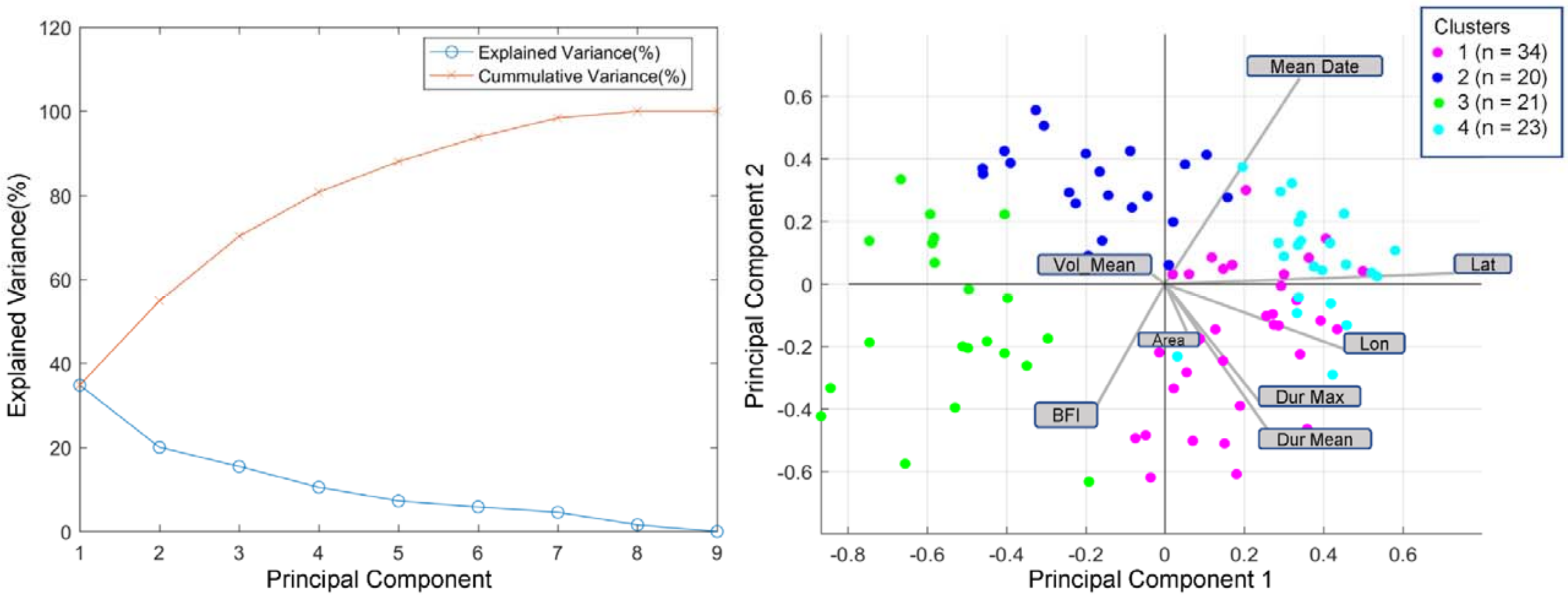

Fig. S3 Identification of drought cluster based on climate and catchment characteristics (a) Explained variance by different principal components (PCs) b) Biplot of the principal components (PCs). Colors indicate the cluster of the catchment. Dur Max, Dur Mean and Vol Mean denote the maximum duration, mean duration and the mean deficit volume respectively. Grey arrows indicate the loadings of the original catchment attributes in the PCA space. The symbol, n in the legend shows the number of sites considered in each cluster. All selected attributes are rescaled and transformed between 0 and 1 using the standard normalization $(\mathrm{X(i)} - \text{minimum}\ (\mathrm{X}))/\mathrm{Range(X)}$, where X indicates selected attributes and $\mathrm{X}(i)$ denotes the attribute value corresponding to each site) before the PCA operation, ensuring the values of the attributes are within the same range.

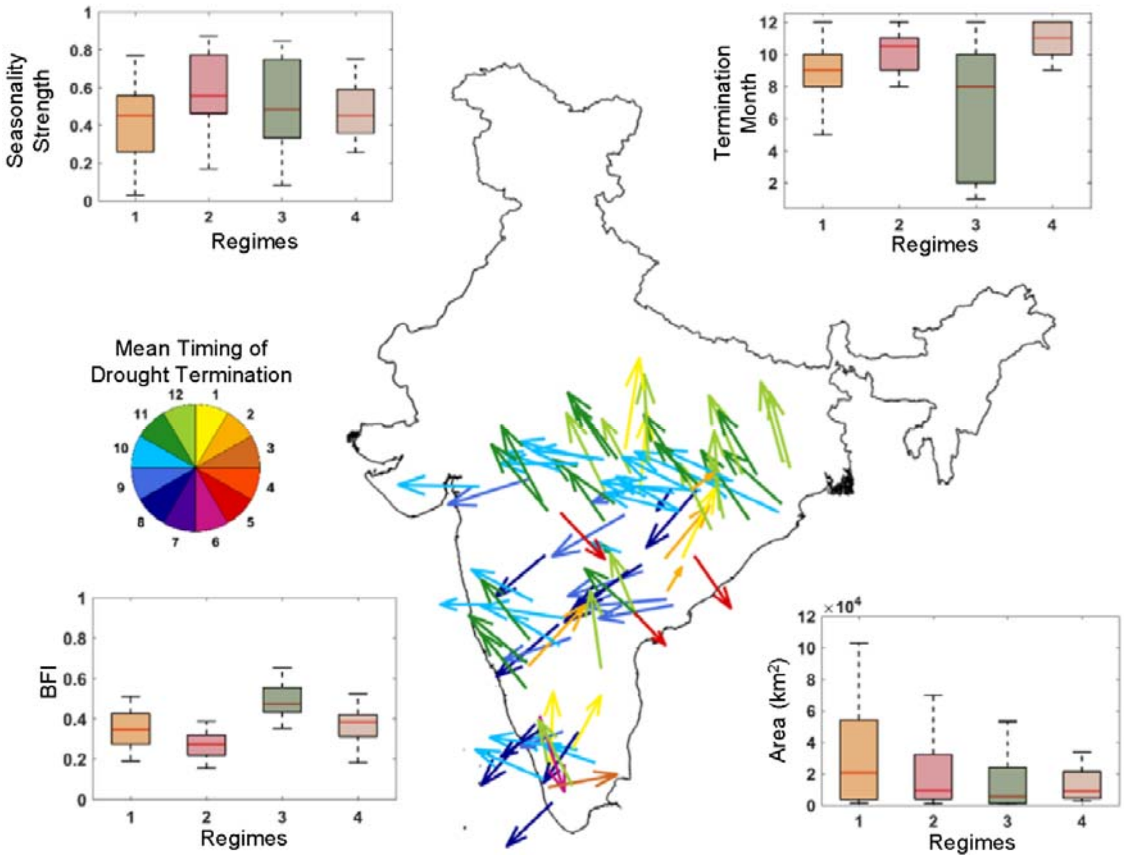

Fig. S4. Spatial distribution of seasonality in drought termination and catchment-specific attributes depicting each region. The shade of the arrow with direction shows the mean timing of drought termination. The length of the arrow shows the circular variance (s^2) for each station; the larger (small) is the size of the arrow, the more (less) is the variability. The boxplot depicts the regional share of seasonality strength (or regularity in drought termination), average termination months, the baseflow index, and catchment area. The shades in the boxplot represent each region. The pie chart (on left) shows the mean timing of drought termination. The shades in the pie chart show the mean termination month: For example, '1' denotes January, whereas '12' indicates December.

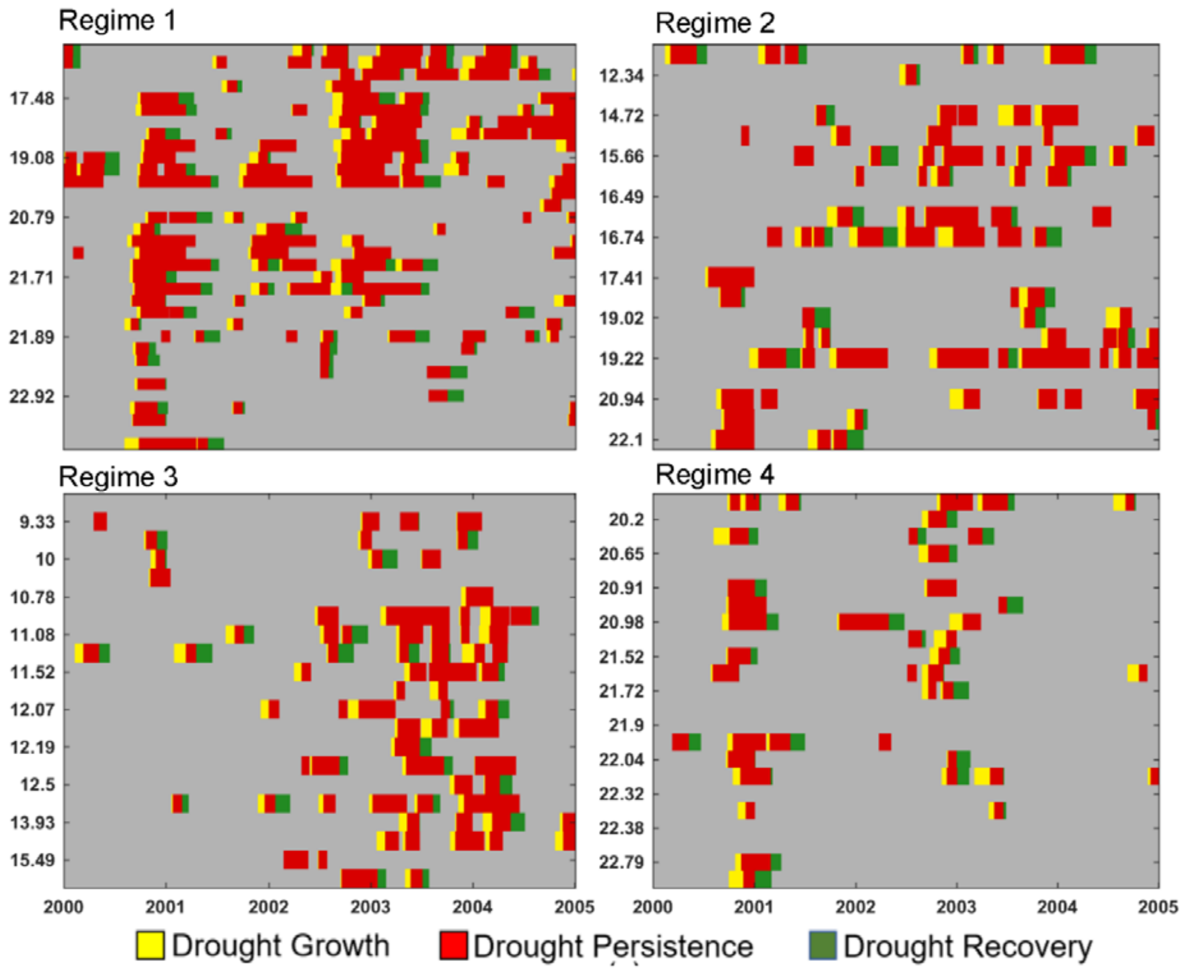

Fig. S5 Hovmöller diagrams (time vs latitude sections) of drought characteristics showing two major historical drought episodes 2000-01 and 2003-04 spanning in the historical time window 2000-05.

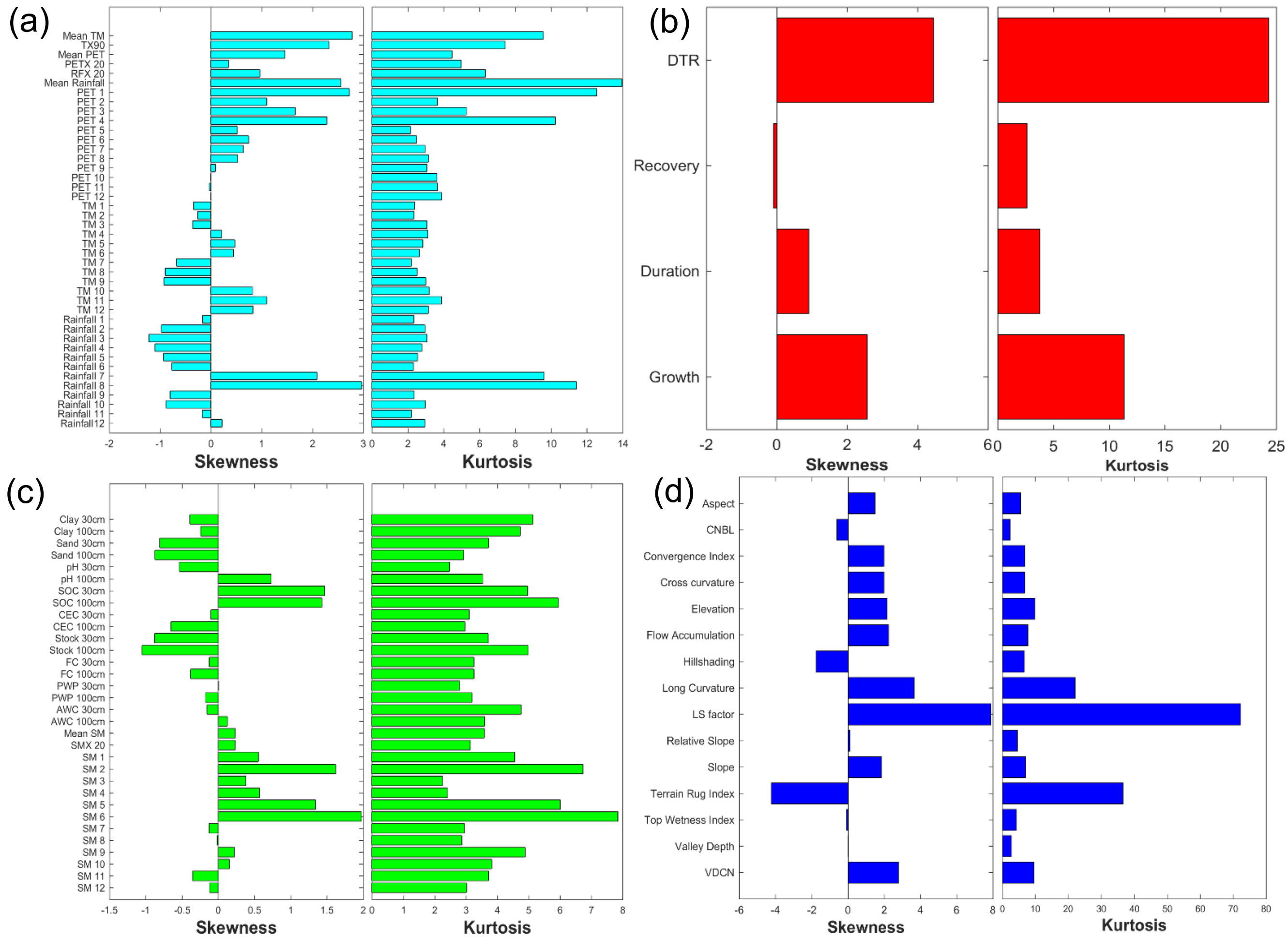

Fig. S6. Skewness and kurtosis values for **(a)** meteorological variables **(b)** drought properties **(c)** soil properties **(d)** catchment characteristics.

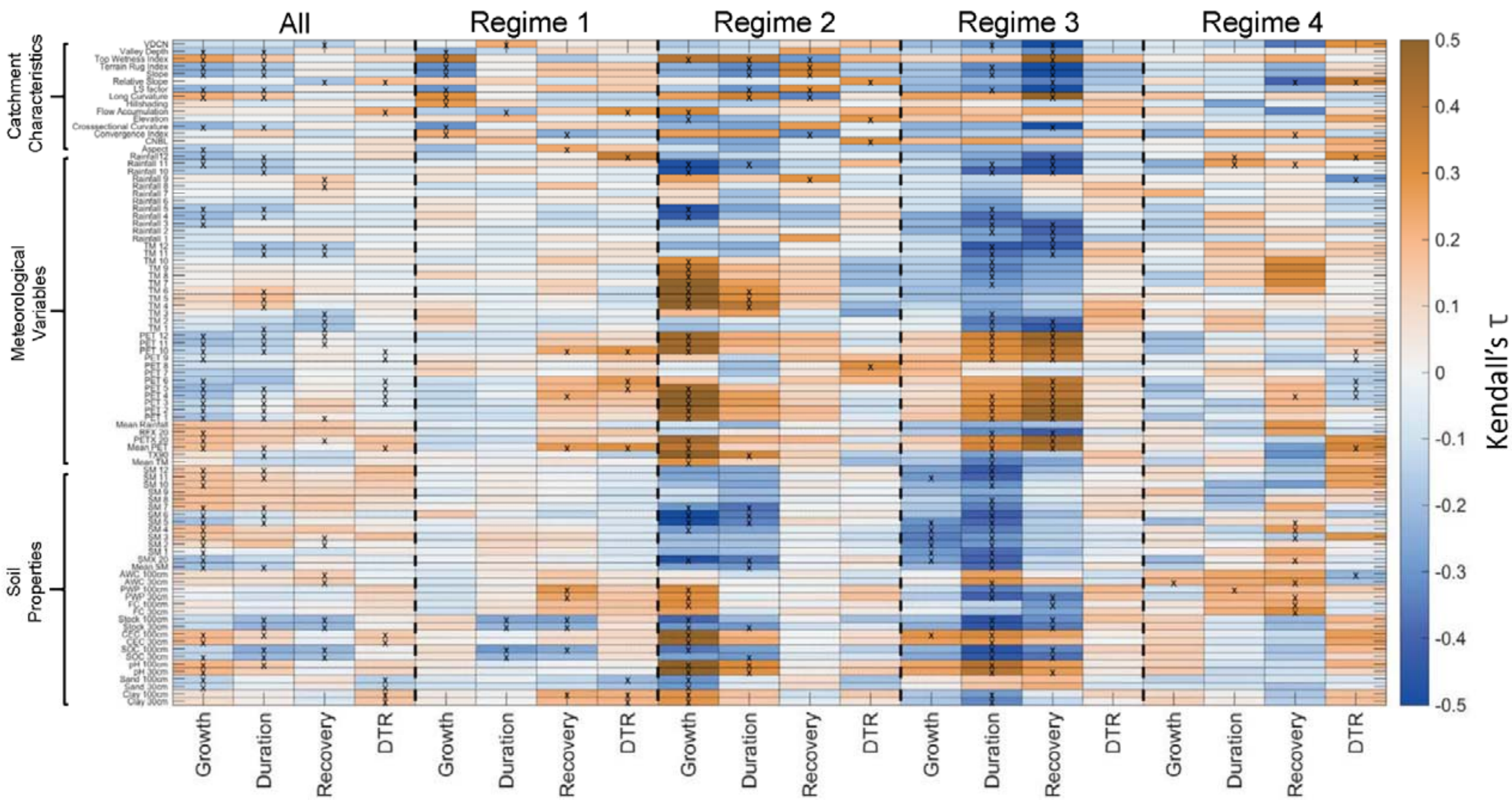

Fig. S7. The Kendall's tau correlation values of 89 covariates as listed in **Table S1** with four different stages of drought namely; growth, duration, recovery and drought termination rate. The crosses show the significant correlation between the variables at 10% significance level.

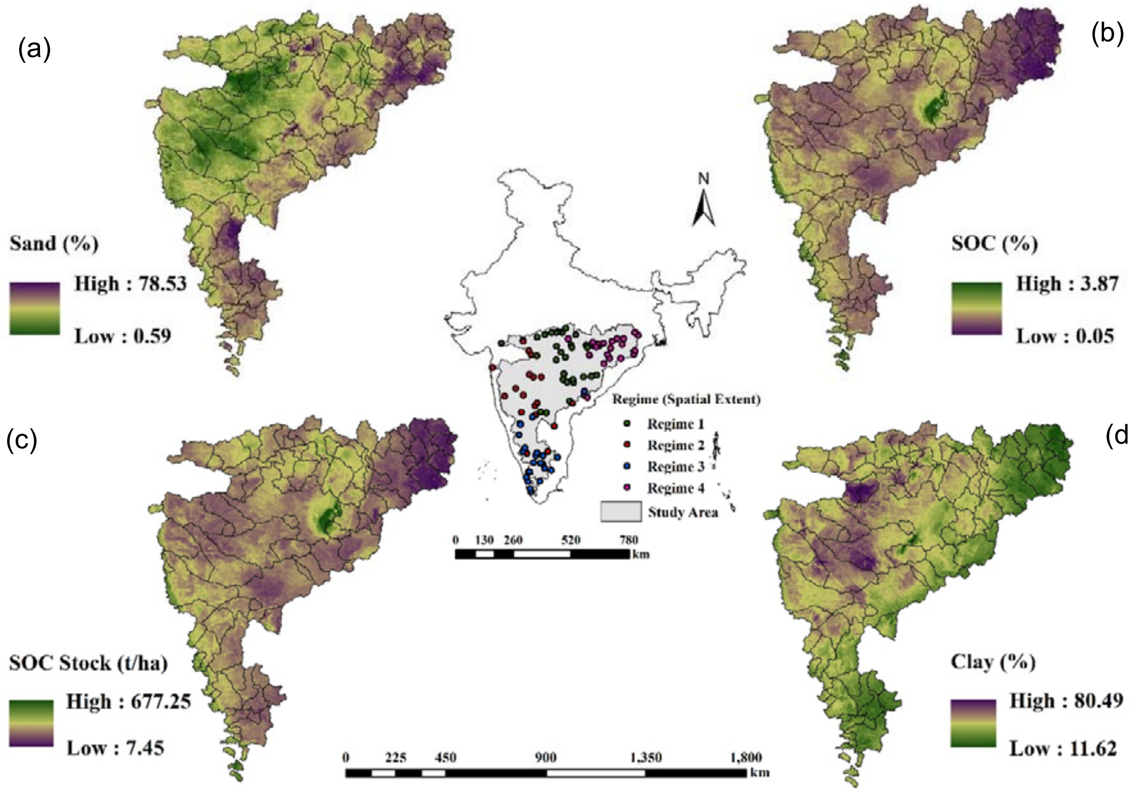

Fig. S8. **Maps for selected soil KDDs as obtained from Boruta feature selection algorithm for various drought stages (a)** average drought growth period; **(b)** average drought duration; **(c)** average drought recovery and **(d)** average drought termination rate attributes across 98 catchments. The India map in the middle shows the delineated drought regimes over the PRB. The map is developed by applying a three-dimensional random forest method coupled with a spatial statistics tool, kriging. The spatial resolution of the map is 500 m.

References

1. Dunn, J. C. Well-separated clusters and optimal fuzzy partitions. *Journal of cybernetics* **4**, 95–104 (1974).
2. Bezdek, J. C. A convergence theorem for the fuzzy ISODATA clustering algorithms. *IEEE transactions on pattern analysis and machine intelligence* 1–8 (1980).
3. Ross, T. J. *Fuzzy logic with engineering applications*. vol. 2 (Wiley Online Library, 2004).
4. Rao, A. R. & Srinivas, V. V. Regionalization of watersheds by hybrid-cluster analysis. *Journal of Hydrology* **318**, 37–56 (2006).
5. Pal, N. R. & Bezdek, J. C. On cluster validity for the fuzzy c-means model. *IEEE Transactions on Fuzzy systems* **3**, 370–379 (1995).